

Quasi-elastic neutrino charged-current scattering cross sections on oxygen

A. V. Butkevich and S. A. Kulagin

Institute for Nuclear Research, Russian Academy of Sciences,

60th October Anniversary Prosp. 7A, Moscow 117312, Russia

The charged-current quasi-elastic scattering of muon neutrinos on oxygen target is computed for neutrino energies between 200 MeV and 2.5 GeV using the relativistic distorted-wave impulse approximation with relativistic optical potential, which was earlier successfully applied to describe electron-nucleus data. We study both neutrino and electron processes and show that the reduced exclusive cross sections for neutrino and electron scattering are similar. The comparison with the relativistic Fermi gas model (RFGM), which is widely used in data analyses of neutrino experiments, shows that the RFGM fails completely when applied to exclusive cross section data and leads to overestimated values of inclusive and total cross sections. We also found significant nuclear-model dependence of exclusive, inclusive and total cross sections for about 1 GeV energy.

PACS numbers: 25.30.-c 25.30.Bf, 25.30.Pt, 13.15.+g

I. INTRODUCTION

The field of neutrino oscillations has been rapidly developing from the observation of anomalies in cosmic rays [1] and solar [2] neutrino data to the cross checks of these anomalies [3, 4] and most recently to terrestrial confirmations of neutrino oscillation hypothesis (Kamland, K2K [5] and MINOS [6]). The next steps in this field would be the precision measurements of observed mass splitting and mixing angles and detailed experimental study of the neutrino mixing matrix.

New, extremely intense neutrino beamlines are in operation or being planned. The data from these experiments will greatly increase statistics. In this situation, statistical uncertainties should be negligible compared to systematic uncertainties (ultimate precisions). An important source of systematic uncertainties is related to nuclear effects in neutrino interactions. Since nuclear targets are used as neutrino detectors, a reliable interpretation of neutrino data requires a detailed knowledge of energy and nuclear dependence of neutrino-nucleus (νA) cross sections. Apparently the uncertainties in neutrino cross sections and nuclear effects produce systematic uncertainties in the extraction of mixing parameters.

Neutrino beams of high intensity cover the energy range from a few hundred MeV to several GeV. In this energy regime, the dominant contribution to neutrino-nucleus cross section comes

from quasi-elastic (QE) reactions and resonance production processes. Unfortunately, the cross section data in the relevant energy range are rather scarce and were taken on targets that are not used in neutrino oscillation experiments (i.e., water, iron, lead or plastic).

A variety of Monte Carlo codes [7] developed to simulate neutrino detector response are based on a simple picture, referred to as Relativistic Fermi Gas Model, in which the nucleus is described as a system of quasi-free nucleons. Comparison with high-precision electron scattering data has shown that the accuracy of predictions of this model (inclusive cross sections) depends significantly on momentum transfer [8]. For inclusive nuclear scattering at sufficiently high momentum transfer ($\gtrsim 500$ MeV/c) the RFGM describes general behavior of cross sections. However, the accuracy of a Fermi gas model becomes poor as momentum transfer decreases (see, e.g., [9]). Furthermore, this model does not account for the nuclear shell structure, and for this reason it fails when applied to exclusive cross sections. There are other important effects beyond the RFGM: the final state interaction (FSI) between the outgoing nucleon and residual nucleus and the presence of strong short-range nucleon-nucleon (NN) correlations, leading to the appearance of high-momentum and high-energy components in the nucleon energy-momentum distribution in the target. In the calculation of Ref. [10] within a plane-wave impulse approximation (PWIA) the nucleon-nucleon correlations were included using description of nuclear dynamics, based on nuclear many-body theory. It was shown that the Fermi gas model overestimates the total νA cross section by as much as 20% at incoming neutrino energies of about 1 GeV. Neutral current and/or charged current (CC) neutrino-nucleus cross sections were studied within the relativistic distorted-wave impulse approximation (RDWIA) in Refs. [11–14] using a relativistic shell model approach. The implementation of the final-state interaction of the ejected nucleon has been done differently. A description of the FSI mechanisms through the inclusion of relativistic optical potential is presented in Refs. [11–13]. In Refs. [11, 12] important FSI effects arise from the use of relativistic optical potential within a relativistic Green’s function approach. In Ref. [13], the final state interaction was included with and without the imaginary part of the optical potential (for inclusive cross section). A reduction of the total cross section of at least 14% was found at neutrino energies of 1 GeV. The relativistic optical potential and relativistic multiple-scattering Glauber approximation were applied in Ref. [14] for the treatment of the FSI effects. Apart from relativistic and the FSI effects. Apart from relativistic and FSI effects, other effects may be important in neutrino-nucleus reactions. In particular, Ref. [15–19] include long-range nuclear correlations (random-phase approximation) and FSI and Coulomb corrections in the calculation of $\nu^{12}\text{C}$ inclusive cross sections near threshold energy.

In this paper, we compute the single-nucleon knockout contribution to the exclusive, inclusive,

and total cross sections of the charged-current QE (anti)neutrino scattering from ^{16}O using different approximations (PWIA and RDWIA) and the Fermi gas model. We employ the LEA code [20] developed for the calculation of contribution from $1p$ - and $1s$ -state nucleons to cross sections in RDWIA. The LEA program, initially designed for computing of exclusive proton-nucleus and electron-nucleus scattering, was successfully tested against $A(e, e'p)$ data [21–24], and we adopt this code for neutrino reactions. In the PWIA, the nuclear differential cross section are described in terms of a nuclear spectral function [25], which includes contributions from nuclear shells as well as from the NN correlations. In our approach, the effect of the NN correlations in the oxygen ground state is evaluated in the PWIA using model nucleon high-momentum component [26, 27]. We propose a way to estimate the FSI effect on the inclusive cross sections in the presence of short-range NN correlations in the ground state. The aim of this work is twofold. First, we compute the RDWIA CC QE neutrino cross sections. Second, we test the RFGM against electron scattering data.

The outline of this paper is the following. In Sec.II we present the formalism for the description of the charged-current lepton-nucleus scattering process. The RDWIA model is briefly introduced in Sec.III. Results of the numerical calculations are presented in Sec.IV. Our conclusions are summarized in Sec.V. In the appendix, we discuss the general Lorentz structure of the hadronic tensor and give expressions for the cross sections of neutrino exclusive scattering used in our analysis.

II. FORMALISM OF QUASI-ELASTIC SCATTERING

We consider electron and neutrino charged-current QE exclusive,

$$l(k_i) + A(p_A) \rightarrow l'(k_f) + N(p_x) + B(p_B), \quad (1)$$

and inclusive,

$$l(k_i) + A(p_A) \rightarrow l'(k_f) + X, \quad (2)$$

scattering off nuclei in a one-photon (W-boson) exchange approximation. Here l labels the incident lepton [electron or muon (anti)neutrino], and l' represents the scattered lepton (electron or muon). Figure 1 defines our conventions for the kinematical variables, where $k_i = (\varepsilon_i, \mathbf{k}_i)$ and $k_f = (\varepsilon_f, \mathbf{k}_f)$ are initial and final lepton momenta, $p_A = (\varepsilon_A, \mathbf{p}_A)$, and $p_B = (\varepsilon_B, \mathbf{p}_B)$ are the initial and final target momenta, $p_x = (\varepsilon_x, \mathbf{p}_x)$ is ejectile nucleon momentum, $q = (\omega, \mathbf{q})$ is the momentum transfer carried by the virtual photon (W-boson), and $Q^2 = -q^2 = \mathbf{q}^2 - \omega^2$ is the photon (W-boson)

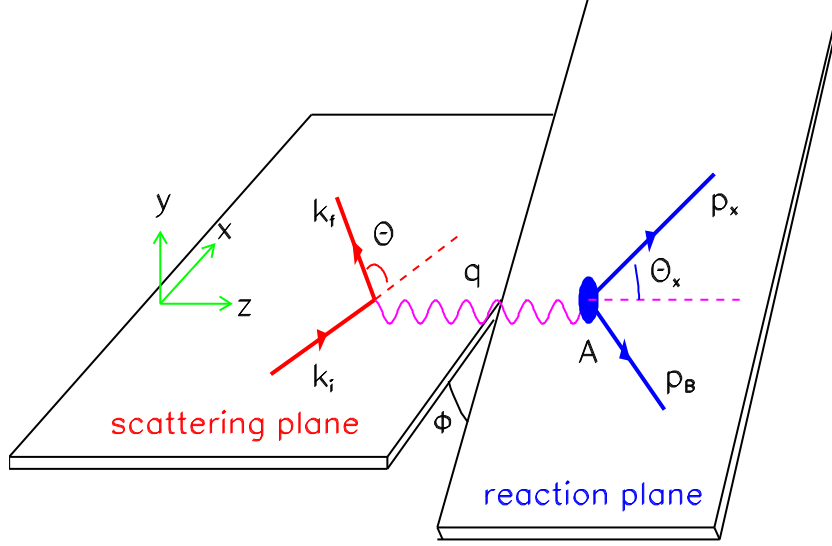


FIG. 1: (Color online) Kinematics for the quasi-elastic lepton-nucleus scattering process.

virtuality. Normalization of states is given by

$$N_i \langle p_i | p'_i \rangle = 2\pi \delta^3(\mathbf{p}_i - \mathbf{p}'_i),$$

where $N_i = m/\varepsilon$ for massive particles, or $N_i = 1/2\varepsilon$ for massless leptons.

A. Quasi-elastic lepton-nucleus cross sections

In the laboratory frame, the differential cross section for exclusive electron (σ^{el}) and (anti)neutrino (σ^{cc}) CC scattering can be written as

$$\frac{d^6 \sigma^{el}}{d\varepsilon_f d\Omega_f d\varepsilon_x d\Omega_x} = \frac{|\mathbf{p}_x| \varepsilon_x}{(2\pi)^3} \frac{\varepsilon_f}{\varepsilon_i} \frac{\alpha^2}{Q^4} L_{\mu\nu}^{(el)} \mathcal{W}^{\mu\nu(el)} \quad (3a)$$

$$\frac{d^6 \sigma^{cc}}{d\varepsilon_f d\Omega_f d\varepsilon_x d\Omega_x} = \frac{|\mathbf{p}_x| \varepsilon_x}{(2\pi)^5} \frac{|\mathbf{k}_f|}{\varepsilon_i} \frac{G^2 \cos^2 \theta_c}{2} L_{\mu\nu}^{(cc)} \mathcal{W}^{\mu\nu(cc)}, \quad (3b)$$

where Ω_f is the solid angle for the lepton momentum, Ω_x is the solid angle for the ejectile nucleon momentum, $\alpha \simeq 1/137$ is the fine-structure constant, $G \simeq 1.16639 \times 10^{-11} \text{ MeV}^{-2}$ is the Fermi constant, θ_C is the Cabbibo angle ($\cos \theta_C \approx 0.9749$), $L^{\mu\nu}$ is the lepton tensor, $\mathcal{W}_{\mu\nu}^{(el)}$ and $\mathcal{W}_{\mu\nu}^{(cc)}$ are correspondingly the electromagnetic and weak CC nuclear tensors which will be discussed below.

For exclusive reactions in which only a single discrete state or narrow resonance of the target is excited, it is possible to integrate over the peak in missing energy and obtain a fivefold differential

cross section of the form

$$\frac{d^5\sigma^{el}}{d\varepsilon_f d\Omega_f d\Omega_x} = R \frac{|\mathbf{p}_x| \tilde{\varepsilon}_x \varepsilon_f \alpha^2}{(2\pi)^3 \varepsilon_i Q^4} L_{\mu\nu}^{(el)} W^{\mu\nu(el)} \quad (4a)$$

$$\frac{d^5\sigma^{cc}}{d\varepsilon_f d\Omega_f d\Omega_x} = R \frac{|\mathbf{p}_x| \tilde{\varepsilon}_x |\mathbf{k}_f| G^2 \cos^2 \theta_c}{(2\pi)^5 \varepsilon_i 2} L_{\mu\nu}^{(cc)} W^{\mu\nu(cc)}, \quad (4b)$$

where R is a recoil factor

$$R = \int d\varepsilon_x \delta(\varepsilon_x + \varepsilon_B - \omega - m_A) = \left| 1 - \frac{\tilde{\varepsilon}_x \mathbf{p}_x \cdot \mathbf{p}_B}{\varepsilon_B \mathbf{p}_x \cdot \mathbf{p}_x} \right|^{-1}, \quad (5)$$

$\tilde{\varepsilon}_x$ is the solution to the equation $\varepsilon_x + \varepsilon_B - m_A - \omega = 0$, where $\varepsilon_B = \sqrt{m_B^2 + \mathbf{p}_B^2}$, $\mathbf{p}_B = \mathbf{q} - \mathbf{p}_x$ and m_A and m_B are masses of the target and recoil nucleus, respectively. Note that the missing momentum is $\mathbf{p}_m = \mathbf{p}_x - \mathbf{q}$.

The lepton tensor can be written as the sum of the symmetric $L_S^{\mu\nu}$ and antisymmetric $L_A^{\mu\nu}$ tensors

$$L^{\mu\nu} = L_S^{\mu\nu} + L_A^{\mu\nu} \quad (6a)$$

$$L_S^{\mu\nu} = 2 \left(k_i^\mu k_f^\nu + k_i^\nu k_f^\mu - g^{\mu\nu} k_i k_f \right) \quad (6b)$$

$$L_A^{\mu\nu} = h 2i \epsilon^{\mu\nu\alpha\beta} (k_i)_\alpha (k_f)_\beta, \quad (6c)$$

where h is $+1$ for positive lepton helicity and -1 for negative lepton helicity, and $\epsilon^{\mu\nu\alpha\beta}$ is the antisymmetric tensor with $\epsilon^{0123} = -\epsilon_{0123} = 1$. For the scattering of unpolarized incident electrons, $L^{\mu\nu(el)}$ only has the symmetric part (6b) and the (anti)neutrino tensor $L^{\mu\nu(cc)}$ involves both the symmetric and the antisymmetric parts. Assuming the reference frame, in which the z axis is parallel to the momentum transfer $\mathbf{q} = \mathbf{k}_i - \mathbf{k}_f$ and the y axis is parallel to $\mathbf{k}_i \times \mathbf{k}_f$, the symmetric components $L_S^{0x}, L_S^{xy}, L_S^{zy}$ and the antisymmetric ones $L_A^{0x}, L_A^{xz}, L_A^{0z}$, as well as those obtained from them by exchanging their indices, vanish. The electromagnetic and the weak CC hadronic tensors, $\mathcal{W}_{\mu\nu}^{(el)}$ and $\mathcal{W}_{\mu\nu}^{(cc)}$, are given by bilinear products of the transition matrix elements of the nuclear electromagnetic or CC operator $J_\mu^{(el)(cc)}$ between the initial nucleus state $|A\rangle$ and the final state $|B_f\rangle$ as

$$\mathcal{W}_{\mu\nu}^{(el)(cc)} = \sum_f \langle B_f, p_x | J_\mu^{(el)(cc)} | A \rangle \langle A | J_\nu^{(el)(cc)\dagger} | B_f, p_x \rangle \delta(\varepsilon_A + \omega - \varepsilon_x - \varepsilon_{B_f}), \quad (7)$$

where the sum is taken over undetected states.

In the inclusive reactions (2) only the outgoing lepton is detected, and the differential cross sections can be written as

$$\frac{d^3\sigma^{el}}{d\varepsilon_f d\Omega_f} = \frac{\varepsilon_f \alpha^2}{\varepsilon_i Q^4} L_{\mu\nu}^{(el)} \overline{W}^{\mu\nu(el)}, \quad (8a)$$

$$\frac{d^3\sigma^{cc}}{d\varepsilon_f d\Omega_f} = \frac{1}{(2\pi)^2} \frac{|\mathbf{k}_f|}{\varepsilon_i} \frac{G^2 \cos^2 \theta_c}{2} L_{\mu\nu}^{(cc)} \overline{W}^{\mu\nu(cc)}, \quad (8b)$$

where $\overline{W}^{\mu\nu}$ is inclusive hadronic tensor. A general covariant form of the hadronic tensors and the results of their contractions with the lepton tensors are given in Appendix A for exclusive lepton scattering (1). Combining Eq.(4a) with Eq.(A3) and Eq.(4b) with Eq.(A7) we obtain the exclusive lepton scattering cross sections in terms of response functions

$$\frac{d^5\sigma^{el}}{d\varepsilon_f d\Omega_f d\Omega_x} = \frac{|\mathbf{p}_x| \tilde{\varepsilon}_x}{(2\pi)^3} \sigma_M R (V_L R_L^{(el)} + V_T R_T^{(el)} + V_{LT} R_{LT}^{(el)} \cos \phi + V_{TT} R_{TT}^{(el)} \cos 2\phi), \quad (9a)$$

$$\begin{aligned} \frac{d^5\sigma^{cc}}{d\varepsilon_f d\Omega_f d\Omega_x} &= \frac{|\mathbf{p}_x| \tilde{\varepsilon}_x}{(2\pi)^5} G^2 \cos^2 \theta_c \varepsilon_f |\mathbf{k}_f| R \{ v_0 R_0 + v_T R_T + v_{TT} R_{TT} \cos 2\phi + v_{zz} R_{zz} \\ &\quad + (v_{xz} R_{xz} - v_{0x} R_{0x}) \cos \phi - v_{0z} R_{0z} + h [v_{yz} (R'_{yz} \sin \phi + R_{yz} \cos \phi) \\ &\quad - v_{0y} (R'_{0y} \sin \phi + R_{0y} \cos \phi) - v_{xy} R_{xy}] \}, \end{aligned} \quad (9b)$$

where

$$\sigma_M = \frac{\alpha^2 \cos^2 \theta / 2}{4\varepsilon_i^2 \sin^4 \theta / 2} \quad (10)$$

is the Mott cross section. The response functions R_i depend on the variables $Q^2, \omega, |\mathbf{p}_x|$, and θ_x . Similarly, the inclusive lepton scattering cross sections reduce to

$$\frac{d^3\sigma^{el}}{d\varepsilon_f d\Omega_f} = \sigma_M (V_L R_L^{(el)} + V_T R_T^{(el)}), \quad (11a)$$

$$\frac{d^3\sigma^{cc}}{d\varepsilon_f d\Omega_f} = \frac{G^2 \cos^2 \theta_c}{(2\pi)^2} \varepsilon_f |\mathbf{k}_f| (v_0 R_0 + v_T R_T + v_{zz} R_{zz} - v_{0z} R_{0z} - h v_{xy} R_{xy}), \quad (11b)$$

where the response functions now depend only on Q^2 and ω .

It is also useful to define a reduced cross section

$$\sigma_{red} = \frac{d^5\sigma}{d\varepsilon_f d\Omega_f d\Omega_x} / K \sigma_{lN}, \quad (12)$$

where $K^{el} = R p_x \varepsilon_x / (2\pi)^3$ and $K^{cc} = R p_x \varepsilon_x / (2\pi)^5$ are phase-space factors for the electron and neutrino scattering, the recoil factor R is given by Eq.(5), and σ_{lN} is the corresponding elementary cross section for the lepton scattering from the moving free nucleon.

B. Nuclear current

Obviously, the determination of the response tensor $W^{\mu\nu}$ requires the knowledge of the nuclear current matrix elements in Eq.(7). We describe the lepton-nucleon scattering in the impulse approximation (IA), assuming that the incoming lepton interacts with only one nucleon, which is

subsequently emitted. The nuclear current is written as the sum of single-nucleon currents. Then, the nuclear matrix element in Eq.(7) takes the form

$$\langle p, B | J^\mu | A \rangle = \int d^3r \exp(i\mathbf{t} \cdot \mathbf{r}) \bar{\Psi}^{(-)}(\mathbf{p}, \mathbf{r}) \Gamma^\mu \Phi(\mathbf{r}), \quad (13)$$

where Γ^μ is the vertex function, $\mathbf{t} = \varepsilon_B \mathbf{q} / W$ is the recoil-corrected momentum transfer, $W = \sqrt{(m_A + \omega)^2 - \mathbf{q}^2}$ is the invariant mass, Φ and $\Psi^{(-)}$ are relativistic bound-state and outgoing wave functions.

For electron scattering, most calculations use the CC2 electromagnetic vertex function for a free nucleon [32]

$$\Gamma^\mu = F_V^{(el)}(Q^2) \gamma^\mu + i\sigma^{\mu\nu} \frac{q_\nu}{2m} F_M^{(el)}(Q^2), \quad (14)$$

where $\sigma^{\mu\nu} = i[\gamma^\mu, \gamma^\nu]/2$, $F_V^{(el)}$ and $F_M^{(el)}$ are the Dirac and Pauli nucleon form factors. Because the bound nucleons are off shell, the vertex Γ^μ in Eq.(13) should be taken for the off-shell region. We employ the de Forest prescription for off-shell vertex [32]

$$\tilde{\Gamma}^\mu = F_V^{(el)}(Q^2) \gamma^\mu + i\sigma^{\mu\nu} \frac{\tilde{q}_\nu}{2m} F_M^{(el)}(Q^2), \quad (15)$$

where $\tilde{q} = (\varepsilon_x - \tilde{E}, \mathbf{q})$ and the nucleon energy $\tilde{E} = \sqrt{m^2 + (\mathbf{p}_x - \mathbf{q})^2}$ is placed on shell. We use the approximation of [33] on the nucleon form factors. The Coulomb gauge is assumed for the single-nucleon current.

The single-nucleon charged current has the $V-A$ structure $J^{\mu(cc)} = J_V^\mu + J_A^\mu$. For a free nucleon vertex function $\Gamma^{\mu(cc)} = \Gamma_V^\mu + \Gamma_A^\mu$, we use the CC2 vector current vertex function

$$\Gamma_V^\mu = F_V(Q^2) \gamma^\mu + i\sigma^{\mu\nu} \frac{q_\nu}{2m} F_M(Q^2), \quad (16)$$

and the axial current vertex function

$$\Gamma_A^\mu = F_A(Q^2) \gamma^\mu \gamma_5 + F_P(Q^2) q^\mu \gamma_5. \quad (17)$$

The weak vector form factors F_V and F_M are related to the corresponding electromagnetic ones for proton $F_{i,p}^{(el)}$ and neutron $F_{i,n}^{(el)}$ by the hypothesis of the conserved vector current (CVC)

$$F_i = F_{i,p}^{(el)} - F_{i,n}^{(el)}. \quad (18)$$

The axial F_A and pseudoscalar F_P form factors in the dipole approximation are parameterized as

$$F_A(Q^2) = \frac{F_A(0)}{(1 + Q^2/M_A^2)^2}, \quad F_P(Q^2) = \frac{2mF_A(Q^2)}{m_\pi^2 + Q^2}, \quad (19)$$

where $F_A(0) = 1.267$, m_π is the pion mass, and $M_A \simeq 1.032$ GeV is the axial mass. We use the de Forest prescription for off-shell extrapolation of $\Gamma^{\mu(cc)}$. Similar to the electromagnetic current, the Coulomb gauge is applied for the vector current J_V .

III. MODEL

In Ref. [34], a formalism was developed for the $A(\vec{e}, e'\vec{N})B$ reaction that describes channel coupling in the FSI of the $N + B$ system. According to Ref. [34], a projection operator P for model space was introduced. In the independent particle shell model (IPSM), the model space for $^{16}\text{O}(e, e'N)$ consists of $1s_{1/2}$, $1p_{3/2}$, and $1p_{1/2}$ nucleon-hole states in ^{15}N and ^{16}O nuclei, for a total of six states. The $1s_{1/2}$ state is regarded as a discrete state even though its spreading width is actually appreciable. For single nucleon knockout, the parentage expansion of the target ground-state can be written as

$$P\Psi_0 = \sum_{\beta\gamma} c_{\beta\gamma} \phi_{\beta\gamma} \Phi_\gamma, \quad (20)$$

where $c_{\beta\gamma}$ is a parentage coefficient and $\phi_{\beta\gamma}$ is an overlap wave function for removal of a nucleon with single-particle quantum number β while leaving the residual nucleus in the state Φ_γ . Assuming that the overlap wave functions are described by the Dirac equation, they can be represented by a Dirac spinor of the form

$$\phi_{\beta\gamma} = \begin{pmatrix} F_{\beta\gamma} \\ iG_{\beta\gamma} \end{pmatrix}. \quad (21)$$

Similarly, for the scattering state

$$P\Psi_\alpha^{(+)} = \sum_\beta \psi_{\alpha\beta}^{(+)} \Phi_\beta \quad (22)$$

is an incoming wave function of the $N + B$ system containing an incident plane wave in the channel α and outgoing spherical waves in all open channels β for $B(N, N')B'$ reaction. The Dirac representation of distorted spinor wave functions is

$$\psi_{\alpha\beta}^{(+)} = N_\alpha \begin{pmatrix} \chi_{\alpha\beta} \\ i\zeta_{\alpha\beta} \end{pmatrix}, \quad (23)$$

where

$$N_\alpha = \sqrt{\frac{E_\alpha + m}{2E_\alpha}} \quad (24)$$

is the asymptotic wave function for channel α normalized to unit flux, and $E_\alpha = \sqrt{k_\alpha^2 + m^2}$ is the channel energy in the barycentric frame (the rest frame of residual nucleus B).

Working in coordinate space, we can write the matrix elements of the current operator (16) for single-nucleon knockout leaving the residual nucleus in asymptotic channel α as follows

$$\langle p, B_\alpha | J^\mu | A \rangle = \sum_{\beta\gamma m_b m'_b} c_{\beta\gamma} \int d^3r \exp(i\mathbf{t} \cdot \mathbf{r}) \langle \bar{\psi}_{\alpha\beta}^{(-)} | \mathbf{r} m_b \rangle$$

$$\times \langle \mathbf{r}m_b | \tilde{\Gamma}^\mu | \mathbf{r}m'_b \rangle \langle \mathbf{r}m'_b | \phi_{\beta\gamma} \rangle. \quad (25)$$

Matrix elements of the single-nucleon current can be expressed in the block-matrix form

$$\tilde{\Gamma}^\mu = \begin{pmatrix} \tilde{\Gamma}_{++}^\mu & \tilde{\Gamma}_{+-}^\mu \\ \tilde{\Gamma}_{-+}^\mu & \tilde{\Gamma}_{--}^\mu \end{pmatrix}, \quad (26)$$

where each of the elements $\langle \mathbf{r}m_b | \tilde{\Gamma}_{\lambda\lambda'}^\mu | \mathbf{r}m'_b \rangle$ is a 2×2 spin matrix, while $\lambda = \{+, -\}$ and $\lambda' = \{+, -\}$ are for the upper (+) and lower (−) Dirac components. Let

$$\langle \mathbf{r}m'_b | \phi_{\beta\gamma} \rangle = \begin{pmatrix} F_{\beta\gamma m'_b}(\mathbf{r}) \\ iG_{\beta\gamma m'_b}(\mathbf{r}) \end{pmatrix} \quad (27)$$

be the bound state overlap wave function and

$$\langle \bar{\psi}_{\alpha\beta}^{(-)} | \mathbf{r}m_b \rangle = N_\alpha \begin{pmatrix} \chi_{\alpha\beta m_b}^{(-)*}(\mathbf{r}) \\ -i\zeta_{\alpha\beta m_b}^{(-)*}(\mathbf{r}) \end{pmatrix} \quad (28)$$

be the Dirac adjoint of time-reversed distorted waves.

For the sake of application to cross section calculations, we consider the relativistic bound-state functions within the Hartree–Bogolioubov approximation in the σ - ω model [35]. In the mean-field approximation, the meson field operators are replaced by their expectation values. The upper and lower radial wave functions in the partial-wave expansion for bound-state wave functions satisfy the usual coupled differential equations

$$\left(\frac{d}{dr} + \frac{\kappa_\gamma + 1}{r} \right) F_{\beta\gamma}(r) = [E_\gamma + m + S_\gamma(r) - V_\gamma(r)] G_{\beta\gamma}(r), \quad (29a)$$

$$\left(\frac{d}{dr} - \frac{\kappa_\gamma + 1}{r} \right) G_{\beta\gamma}(r) = [-E_\gamma + m + S_\gamma(r) + V_\gamma(r)] F_{\beta\gamma}(r), \quad (29b)$$

where S_γ and V_γ are spherical scalar and vector potentials, and $j_\gamma = |\kappa_\gamma| - 1/2$ is the total angular momentum. Note that these potentials generally depend on the state of the residual nucleus that is marked by subscript γ . The radial wave functions are normalized as

$$\int dr \, r^2 \left(|F_{\beta\gamma}|^2 + |G_{\beta\gamma}|^2 \right) = 1. \quad (30)$$

The missing momentum distribution is determined by the wave functions in momentum space

$$\tilde{F}_{\beta\gamma}(p) = \int dr \, r^2 j_{l_\gamma}(pr) F_{\beta\gamma}(r), \quad (31a)$$

$$\tilde{G}_{\beta\gamma}(p) = \int dr \, r^2 j_{l'_\gamma}(pr) G_{\beta\gamma}(r), \quad (31b)$$

where $j_l(x)$ is the Bessel function of order l and $l'_\gamma = 2j_\gamma - l_\gamma$. If only a single state of residual nucleus is considered, or if relativistic potentials S and V weakly depend on the state γ of residual nucleus, the relativistic momentum distribution can be written in terms of Eq.(30) as

$$P_\beta(p_m) = \frac{|c_\beta|^2}{2\pi^2} \left(|\tilde{F}_\beta(p_m)|^2 + |\tilde{G}_\beta(p_m)|^2 \right). \quad (32)$$

In this work, the current operator CC2 and the bound-nucleon wave functions [36] (usually referred to as NLSH) are used in the numerical analysis. Note that the calculation of the bound-nucleon wave function for $1p_{3/2}$ state includes the incoherent contribution of the unresolved $2s_{1/2}d_{5/2}$ doublet. The wave functions for these states were taken from the parameterization of Ref. [37]. We use also the following values of normalization factors $S_\alpha = |c_\alpha|^2$ relative to the full occupancy of ^{16}O : $S(1p_{3/2}) = 0.66$, $S(1p_{1/2}) = 0.7$ [23], and $S(1s_{1/2}) = 1$.

The distorted wave functions are evaluated using a relativized Schrödinger equation for upper components of Dirac wave functions. For simplicity, we consider a single-channel Dirac equation

$$[\alpha \cdot \mathbf{p} + \beta(m + S)] \psi = (E - V)\psi, \quad (33)$$

where

$$\psi(\mathbf{r}) = \begin{pmatrix} \psi_+(\mathbf{r}) \\ \psi_-(\mathbf{r}) \end{pmatrix} \quad (34)$$

is the four-component Dirac spinor. Using the direct Pauli reduction method [38, 39], the system of two coupled first-order radial Dirac equations can be reduced to a single second-order equation

$$[\nabla^2 + k^2 - 2\mu(U^C + U^{LS}\mathbf{L} \cdot \boldsymbol{\sigma})] \xi = 0, \quad (35)$$

where ξ is a two-component Pauli spinor. Here k is the relativistic wave number, μ is the reduced mass of the scattering state, and

$$U^C = \frac{E}{\mu} \left[V + \frac{m}{E} S + \frac{S^2 - V^2}{2E} \right] + U^D, \quad (36a)$$

$$U^D = \frac{1}{2\mu} \left[-\frac{1}{2r^2 D} \frac{d}{dr} (r^2 D') + \frac{3}{4} \left(\frac{D'}{D} \right)^2 \right], \quad (36b)$$

$$U^{LS} = -\frac{1}{2\mu r} \frac{D'}{D}, \quad (36c)$$

$$D = 1 + \frac{S - V}{E + m}. \quad (36d)$$

where $D' = dD/dr$, and $D(r)$ is known as the Darwin nonlocality factor, and U^C and U^{LS} are the central and spin-orbit potentials. The upper and lower components of the Dirac wave functions

are then obtained using

$$\psi_+ = D^{1/2}\xi, \quad (37a)$$

$$\psi_- = \frac{\boldsymbol{\sigma} \cdot \mathbf{p}}{E + m + S - V} \psi_+. \quad (37b)$$

Assuming a similar relationship for the coupled-channel case, i.e.,

$$\zeta_{\alpha\beta}^{(+)}(\mathbf{r}) = \frac{\boldsymbol{\sigma} \cdot \mathbf{p}}{E_\beta + m + S_\beta - V_\beta} \chi_{\alpha\beta}^{(+)}(\mathbf{r}), \quad (38)$$

the lower components of the radial wave functions in the partial-wave expansion for distorted waves (31) can be approximated as

$$\zeta_{\alpha\beta}^{(+)}(r) = (E_\beta + m + S_\beta - V_\beta)^{-1} \left(\frac{d}{dr} + \frac{\kappa_\beta}{r} \right) \chi_{\alpha\beta}^{(+)}(r). \quad (39)$$

We use the LEA program [20] for the numerical calculation of the distorted wave functions with the EDAD1 SV relativistic optical potential [40]. This code employs an iteration algorithm to solve the relativized Schrödinger equation.

A complex relativistic optical potential with a nonzero imaginary part generally produces an absorption of flux. For the exclusive channel, this reflects the coupling between different open reaction channels. However, for the inclusive reaction the total flux must conserve. Currently there is no fully consistent solution to this problem, and different approaches are used. The Green's function approach, where the FSI effect in inclusive reactions is treated by means of a complex optical potential and the total flux is conserved, is presented in Refs.[11, 41]. To demonstrate the effect of the optical potential on the inclusive reactions, the results obtained in this approach were compared with those obtained with the same potential but with the imaginary part set to 0. It was shown that the inclusive CC neutrino cross sections calculated with only the real part of optical potential are almost identical to those of the Green's function approach [11, 12]. A similar approximation was used also in Ref. [13] to study the FSI effect on the inclusive cross section. In this work, in order to calculate the inclusive and total cross sections, we use the approach in which only the real part of the optical potential EDAD1 is included. Then the contribution of the $1p$ and $1s$ states to the inclusive cross section can be obtained by integrating the exclusive cross sections (11) over the azimuthal angle ϕ and missing momentum, that is, p_m

$$\left(\frac{d^3\sigma}{d\varepsilon_f d\Omega_f} \right)_{\text{RDWIA}} = \int_0^{2\pi} d\phi \int_{p_{\min}}^{p_{\max}} dp_m \frac{p_m}{p_x |\mathbf{q}|} R_c \times \left(\frac{d^5\sigma}{d\varepsilon_f d\Omega_f d\Omega_x} \right)_{\text{RDWIA}},$$

where $p_m = |\mathbf{p}_m|$, $p_x = |\mathbf{p}_x|$, $\mathbf{p}_m = \mathbf{p}_x - \mathbf{q}$, and

$$\cos \theta_x = \frac{\mathbf{p}_x^2 + \mathbf{q}^2 - \mathbf{p}_m^2}{2p_x |\mathbf{q}|}, \quad (40a)$$

$$R_c = 1 + \frac{\varepsilon_x}{2p_x^2 \varepsilon_B} (\mathbf{p}_x^2 + \mathbf{q}^2 - \mathbf{p}_m^2). \quad (40b)$$

The integration limits p_{min} and p_{max} are given in Ref. [27]. The effect of the FSI on the inclusive cross section can be evaluated using the ratio

$$\Lambda(\varepsilon_f, \Omega_f) = \left(\frac{d^3\sigma}{d\varepsilon_f d\Omega_f} \right)_{\text{RDWIA}} / \left(\frac{d^3\sigma}{d\varepsilon_f d\Omega_f} \right)_{\text{PWIA}}, \quad (41)$$

where $(d^3\sigma/d\varepsilon_f d\Omega_f)_{\text{PWIA}}$ is the result obtained in the PWIA.

According to data from the Thomas Jefferson National Accelerator Facility (JLab) [23], the occupancy of the IPSM orbitals of ^{16}O is approximately 75% on average. In this paper, we assume that the missing strength can be attributed to the short-range NN correlations in the ground state. To estimate this effect in the inclusive cross sections, we consider a phenomenological model. This model incorporates both the single particle nature of the nucleon spectrum at low energy and high-energy and high-momentum components due to NN correlations. The high-momentum part P_{HM} of the spectral function is determined by excited states with one or more nucleons in continuum. The detailed description of this model is given in Refs.[26, 27].

In our calculations the spectral function P_{HM} incorporates 25% of the total normalization of the spectral function. The FSI effect for the high-momentum component is estimated by scaling the PWIA result $(d^3\sigma/d\varepsilon_f d\Omega_f)_{\text{HM}}$ with $\Lambda(\varepsilon_f, \Omega_f)$ function (41). Then the total inclusive cross section can be written as

$$\frac{d^3\sigma}{d\varepsilon_f d\Omega_f} = \left(\frac{d^3\sigma}{d\varepsilon_f d\Omega_f} \right)_{\text{RDWIA}} + \Lambda(\varepsilon_f, \Omega_f) \left(\frac{d^3\sigma}{d\varepsilon_f d\Omega_f} \right)_{\text{HM}}. \quad (42)$$

More details about calculation of the $(d^3\sigma/d\varepsilon_f d\Omega_f)_{\text{HM}}$ can be found in Ref. [8].

IV. RESULTS

The LEA code was successfully tested against $A(e, e'p)$ data [22–24]. In Ref. [23] the uncertainty in the normalization factors S_α was estimated to be about $\pm 15\%$. For illustration, Fig. 2 shows the measured JLab [23] and Saclay [42] differential cross sections for the removal of protons from the $1p$ shell of ^{16}O as functions of missing momentum p_m as compared with LEA code calculations. The reduced cross sections together with Saclay [43] and NIKHEF [44] data are shown in Fig. 3. It should be noted that negative values of p_m correspond to $\phi = \pi$ and positive ones to $\phi = 0$. The cross sections were calculated using the kinematic conditions with the normalization factors of data examined [23]. Also shown in Figs. 2 and 3 are the results obtained in the PWIA and RFGM (with the Fermi momentum $p_F = 225$ MeV/c, binding energy $\epsilon = 27$ MeV and including the Pauli

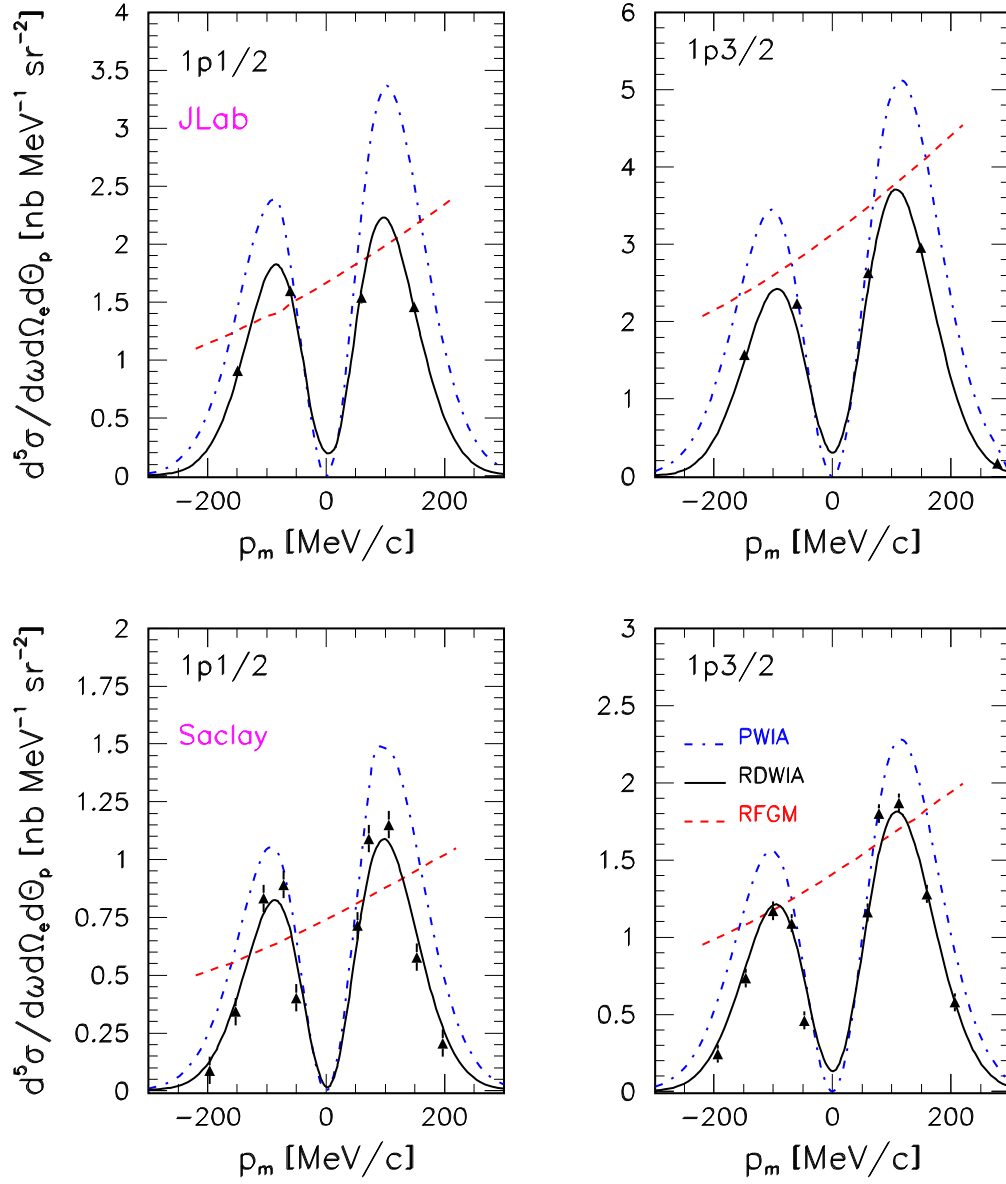


FIG. 2: (Color online) Calculations compared with measured differential exclusive cross section data for the removal of protons from the $1p$ shell of ^{16}O as a function of missing momentum. Upper panels: JLab data [23] for beam energy $E_{\text{beam}}=2.442$ GeV, proton kinetic energy $T_p=427$ MeV, and $Q^2=0.8$ GeV². Lower panels: Saclay data [42] for $E_{\text{beam}}=580$ MeV, $T_p=160$ MeV, and $Q^2=0.3$ GeV².

blocking factor). Apparently the PWIA and RFGM overestimate the values of the cross sections, because the FSI effects are neglected. Moreover, the RFGM predictions are completely off of the exclusive data. This is because of the uniform momentum distribution of the Fermi gas model.

The reduced cross sections for the removal of nucleons from $1p$ shell in $^{16}\text{O}(e, e'p)^{15}\text{N}$,

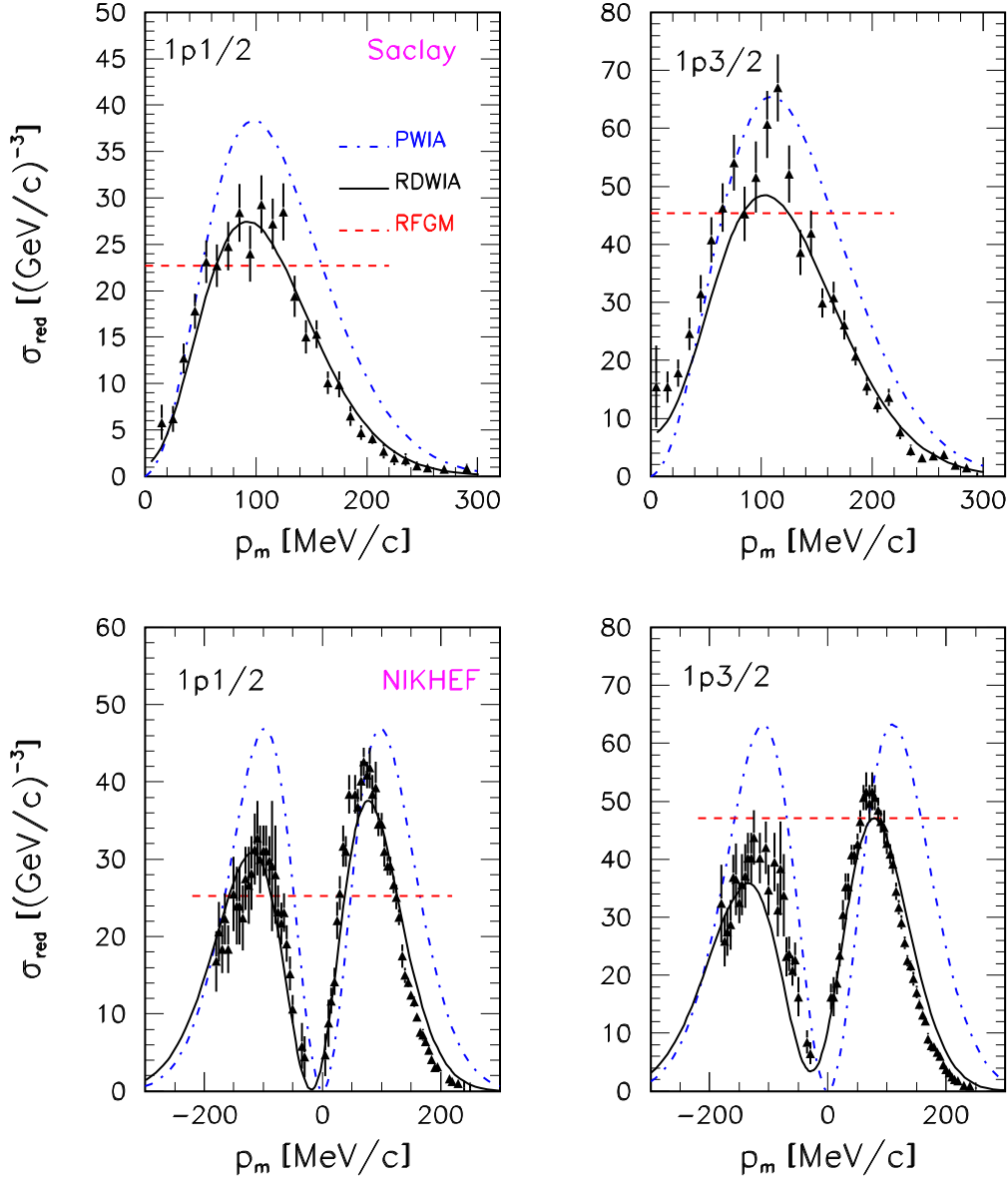


FIG. 3: (Color online) Calculations compared with measured reduced exclusive cross section data for the removal of protons from the $1p$ shell of ^{16}O as a function of missing momentum. Upper panels: Saclay data [43] for beam energy $E_{\text{beam}}=500$ MeV, proton kinetic energy $T_p=100$ MeV, and $Q^2=0.3$ GeV 2 . Lower panels: NIKHEF data [44] for $E_{\text{beam}}=521$ MeV, $T_p=96$ MeV, and Q^2 is varied.

$^{16}\text{O}(\nu, \mu^- p)^{15}\text{O}$, and $^{16}\text{O}(\bar{\nu}, \mu^+ n)^{15}\text{N}$ reactions are shown in Fig. 4 as functions of p_m together with Saclay [43] and NIKHEF data. There is an overall good agreement between calculated cross sections, but the value of electron cross sections at the maximum is systematically higher (less than 10%) than (anti)neutrino ones with the exception of the $1p_{1/2}$ state for Saclay kinematics. The

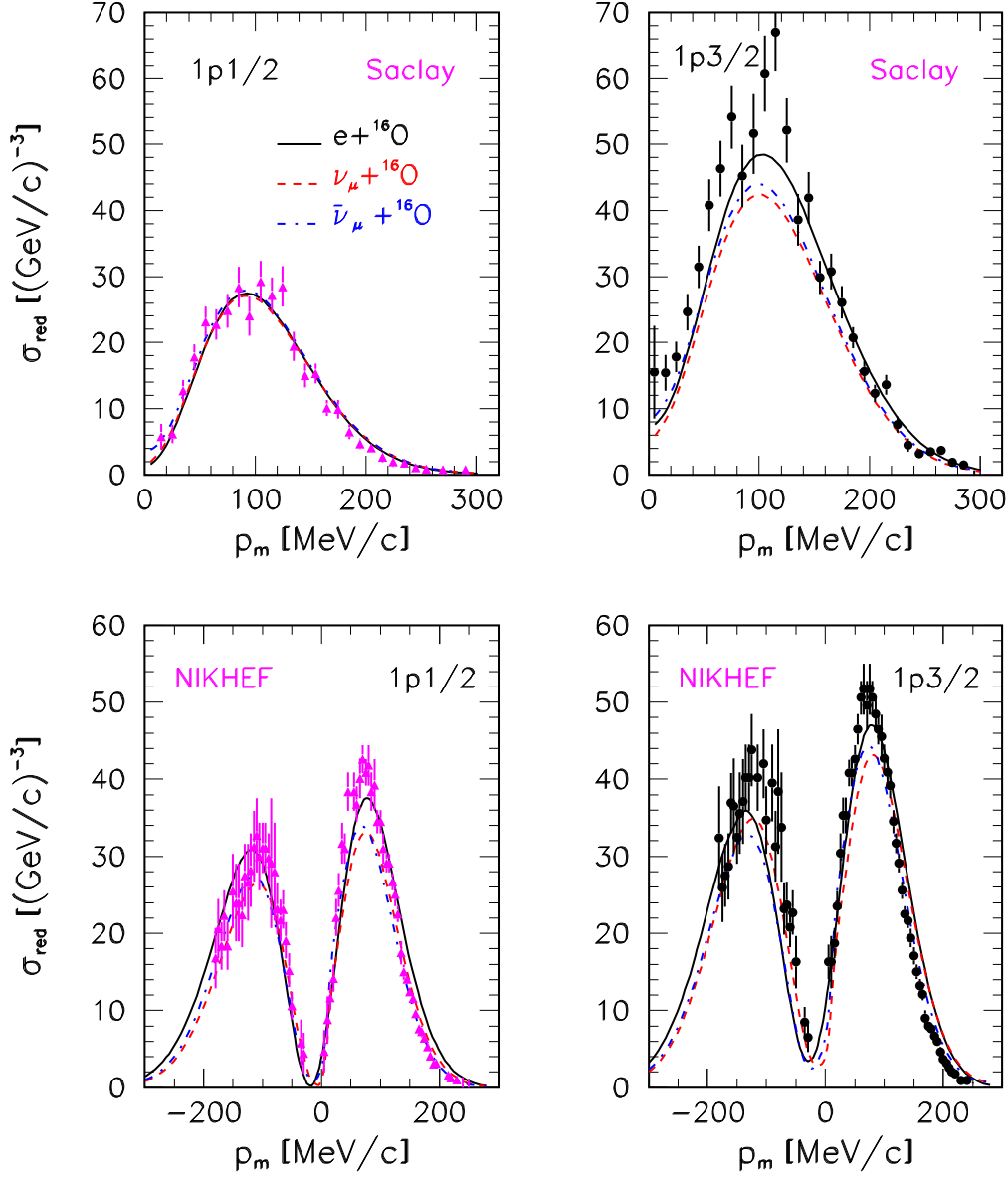


FIG. 4: (Color online) Comparison of the RDWIA electron, neutrino and antineutrino reduced cross sections for the removal of nucleons from the $1p$ shell of ^{16}O for Saclay [43] and NIKHEF [44] kinematics as functions of p_m .

small difference between neutrino and antineutrino reduced cross sections is due to the difference in the FSI of proton and neutron with the residual nucleus.

The differential and reduced electron and (anti)neutrino exclusive cross sections for the removal of nucleons from $1p$ and $1s$ states were calculated for JLab and Saclay [42] kinematics. The results are shown in Fig. 5 together with the RFGM calculations. There is a good agreement between all

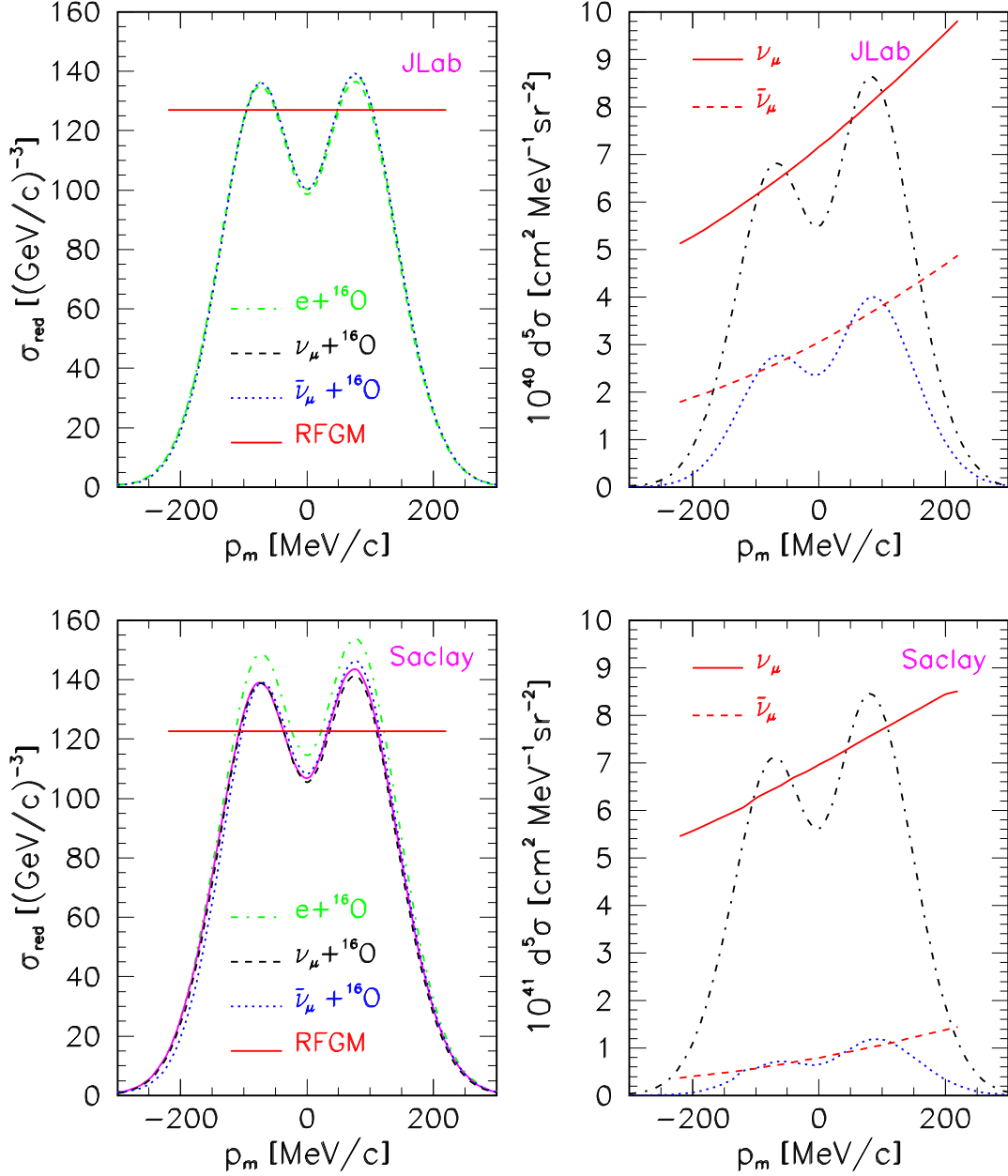


FIG. 5: (Color online) Comparison of the RDWIA and the RFGM calculations for electron, neutrino and antineutrino reduced (left panels) and differential (right panels) cross sections for the removal of nucleons from $1p$ and $1s$ shells of ^{16}O as functions of missing momentum. The cross sections were calculated for the JLab [23] and Saclay [42] kinematics. In the left panels, the RDWIA calculations are shown for electron scattering (dashed-dotted line) and neutrino (dashed line) and antineutrino (dotted line) scattering; and the RFGM results are shown for the reduced cross sections (solid line). In the right panels, the RFGM calculations are shown for the neutrino (solid line) and antineutrino (dashed line) differential cross sections; and the RDWIA results are shown for the neutrino (dashed-dotted line) and antineutrino (dotted line) differential cross sections.

cross sections calculated in the RDWIA for JLab kinematics. The difference between the electron and (anti)neutrino reduced cross sections calculated for Saclay kinematics is less than 10%. This can be attributed to Coulomb distortion upon the electron wave function which is usually described in the effective momentum approximation (EMA) [45]. In the EMA, the electron Coulomb wave function is replaced by a plane wave with effective momentum whose value is larger than the value of electron momentum at infinity, because of Coulomb attraction. This effect weakens as the beam energy increases, and for this reason this effect is more significant at Saclay kinematics ($E_{\text{beam}} = 500$ MeV) than at JLab kinematics ($E_{\text{beam}} = 2442$ MeV). Note that the RFGM results demonstrate absolutely different behavior.

To test our approach, we calculated the inclusive $^{16}\text{O}(e, e')$ cross sections and compared them with SLAC data [46] and Frascati data [47]. Figures 6 and 7 show measured inclusive cross sections as functions of energy transfer, or the invariant mass W as compared with the RDWIA, PWIA, and RFGM calculations. We note that relative to the PWIA results, the generic effect of the FSI with the real part of the optical potential is to reduce the cross section value around the peak and to shift the peak toward the lower value energy transfer. The inclusion of the high-momentum component increases the inclusive cross section in the high-energy transfer region and improves the agreement with data. For the RDWIA results, the difference between the calculated and measured cross sections at the maximum are less than $\pm 10\%$, with the exception of Frascati data for $E_e = 700$ MeV. For the RFGM results, these differences decrease with $|\mathbf{q}|$ from about 22% at $|\mathbf{q}| \approx 330$ MeV/c down to $\approx 2\%$ at $|\mathbf{q}| \approx 640$ MeV/c. These results demonstrate a strong nuclear-model dependence of the inclusive cross sections at low momentum transfer. This dependence weakens as $|\mathbf{q}|$ increases, almost disappearing at $|\mathbf{q}| \geq 500$ MeV/c. The results for $(e, e'N)$ channel indicate that at least 50% of the inclusive cross section can be attributed to the single-step nucleon knockout.

The inclusive neutrino and antineutrino cross sections for energies $E_\nu = 300, 500, 700,$ and 1000 MeV are presented in Figs. 8 and 9, which show $d\sigma/dE_\mu$ as a function of muon energy. Here, the results obtained in the RDWIA with the real optical potential (RDWIA ROP) are compared with the inclusive cross sections calculated in the PWIA, RFGM, and RDWIA with complex optical potential (RDWIA EX). The cross section values obtained in the RFGM are higher than the ones obtained within the RDWIA ROP. For neutrino (antineutrino) cross sections in the region close to the maximum, this discrepancy is about 35%(60%) for $E_\nu = 300$ MeV and 30%(40%) for $E_\nu = 1000$ MeV. The contribution of $(\nu, \mu N)$ channels to the inclusive cross sections is about 60%.

The total cross sections $\sigma(E_\nu)$ together with data [48, 49] are presented in Fig. 10 as functions

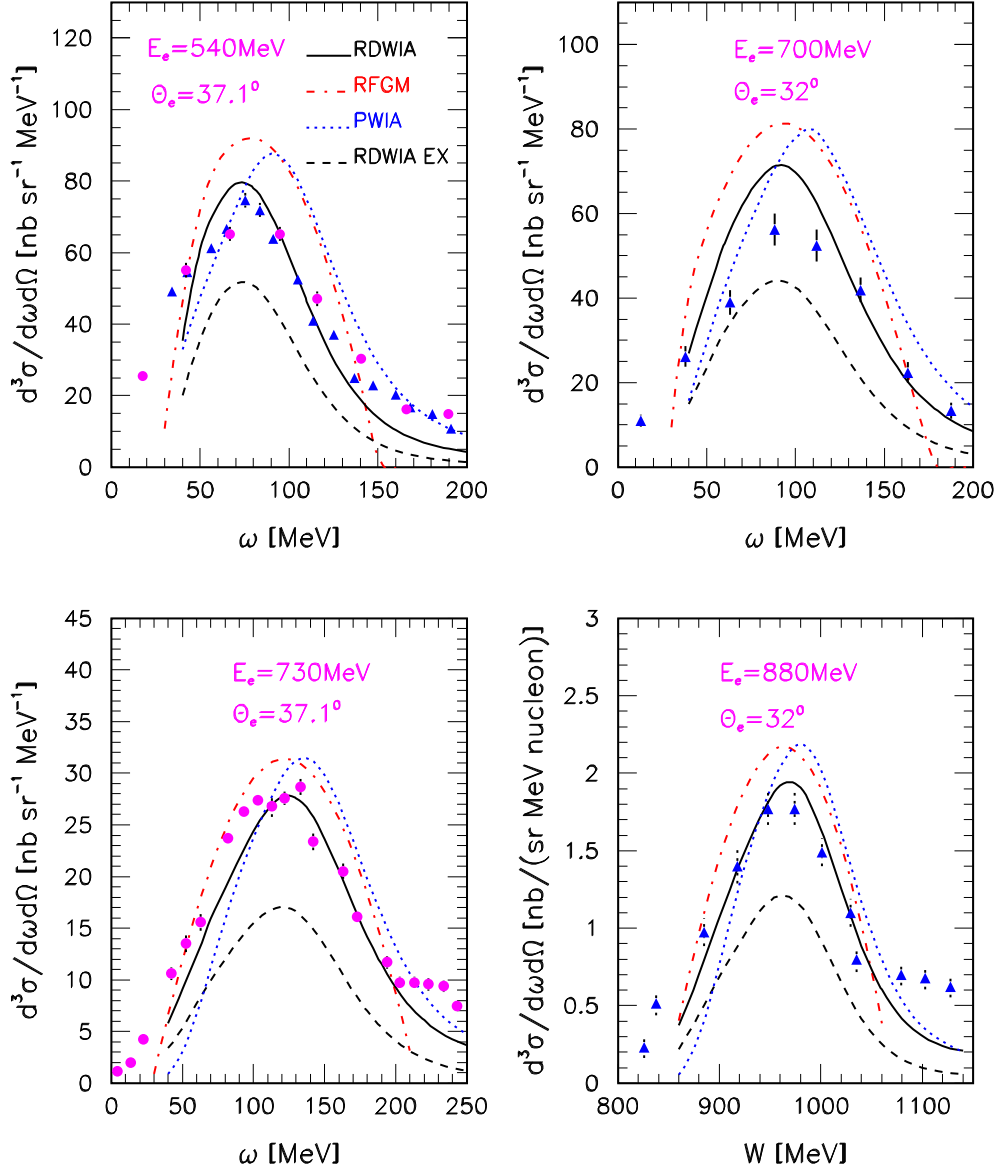


FIG. 6: (Color online) Inclusive cross section vs energy transfer ω or invariant mass W for electron scattering on ^{16}O . The data are from Ref.[46] (SLAC, filled circles) and Ref.[47] (Frascati, filled triangles). SLAC data are for electron beam energy $E_e=540, 730$ MeV and scattering angle $\theta_e=37.1^\circ$. Frascati data are for $E_e=540$ MeV and $\theta_e=37.1^\circ$, $E_e=700, 880$ MeV and $\theta_e=32^\circ$. As shown in the key, cross sections were calculated with the RDWIA, PWIA, RFGM and RDWIA with complex optical potential (EX).

of the incident neutrino energy. The upper panel shows the total cross sections for ^{16}O (ν, μ^-) reaction calculated in the RDWIA with the real part of EDAD1 potential, and the lower panel shows the total cross sections for the $^{16}\text{O}(\nu_\mu, \mu^- p)$ channel. Also shown are the results obtained in Refs. [11, 13] with the NLSH bound nucleon wave functions, dipole approximation of the nucleon

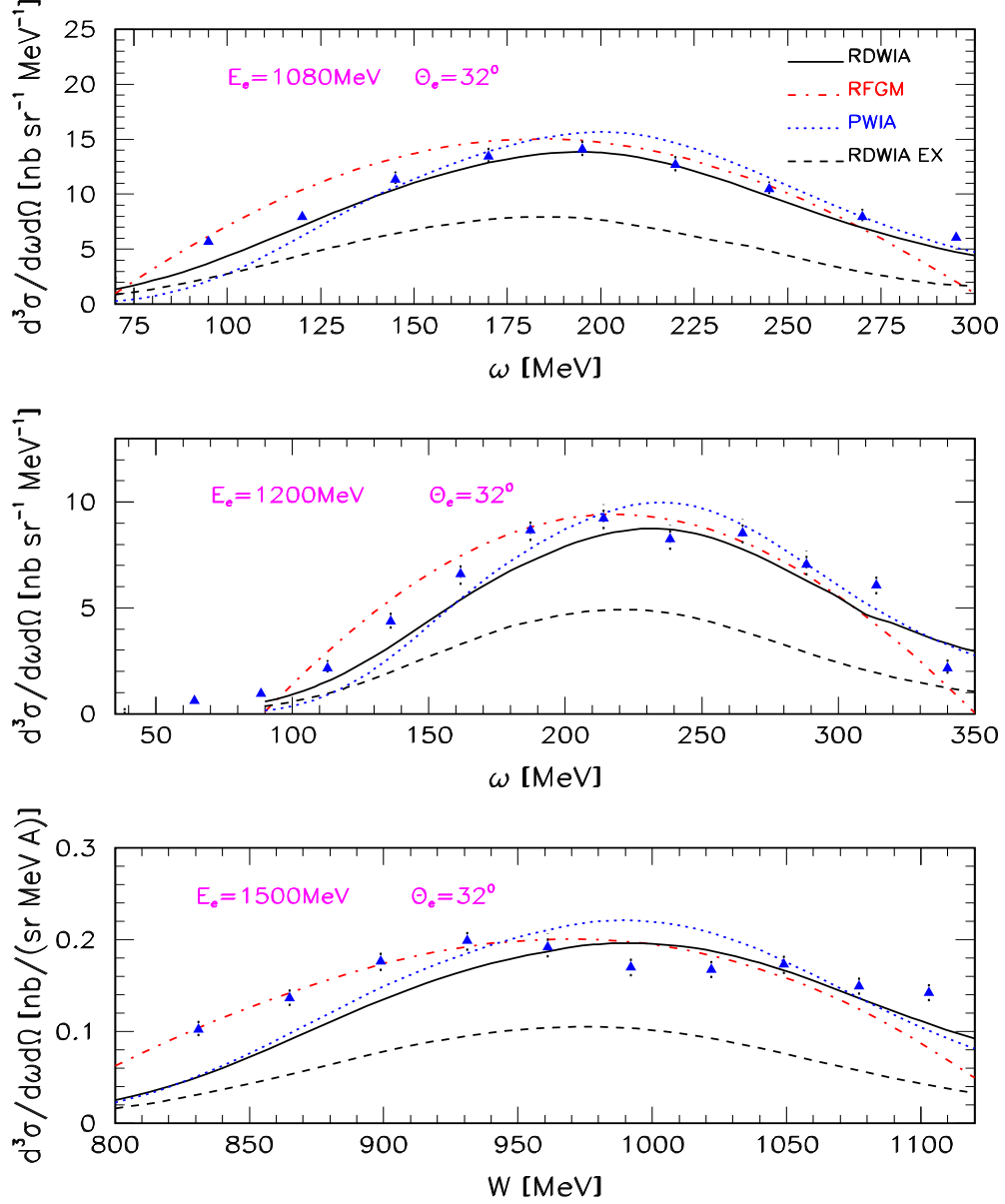


FIG. 7: (Color online) Same as Fig. 6, but the data are from Ref.[47] for electron beam energy $E_e=1080$, 1200, and 1500 MeV and scattering angle $\theta_e=32^\circ$.

form factors, EDAD1 optical potential and neglecting the NN correlation contributions. The cross sections are scaled with the number of neutrons in the target.

Our values of $(\nu, \mu^-)[(\nu_\mu, \mu^- p)]$ cross sections are systematically larger than those from Ref. [11]. The discrepancy increases with energy from about 17%(7%) for $E_\nu = 300$ MeV up to 28%(20%) for $E_\nu = 1000$ MeV. On the other hand, our cross sections are lower than those from Ref. [13], and the discrepancy decreases with energy from 37%(15%) for $E_\nu = 300$ MeV upto 15% (7%) down

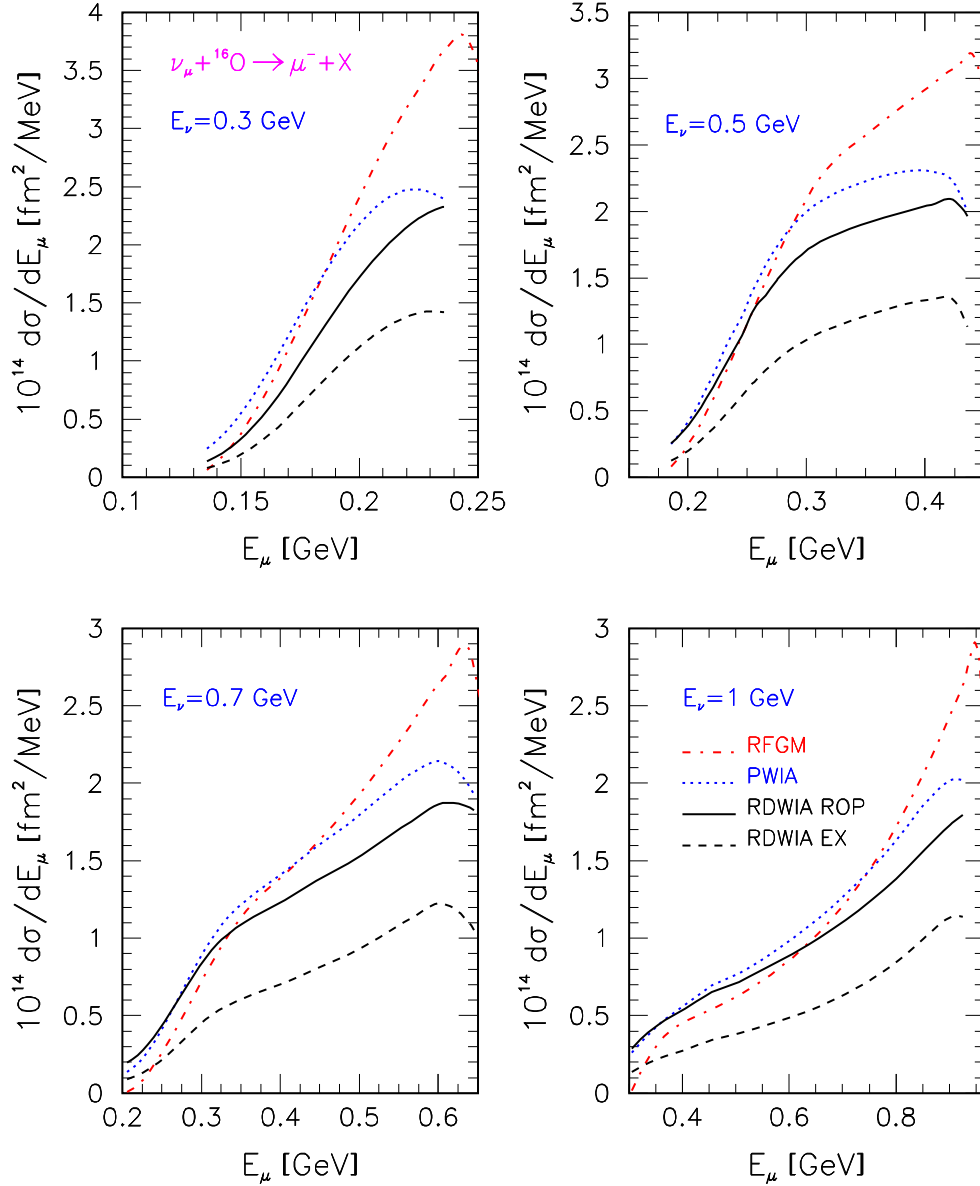


FIG. 8: (Color online) Inclusive cross section vs the muon energy for neutrino scattering on ^{16}O and for the four values of incoming neutrino energy: $E_\nu=0.3, 0.5, 0.7$, and 1 GeV.

to $E_\nu = 1000$ MeV. To study the NN correlation effect, we calculated the total cross sections without the high-momentum contribution, i.e., with $S_\alpha = 1$ for all bound nucleon states, similar to Refs [11, 13]. The results are shown in Fig. 10. Apparently, the NN correlation effect reduces the total cross section. The difference between the results obtained with and without the high-momentum component contribution decreases with neutrino energy from about 20% for $E_\nu = 200$ MeV down to $\approx 8\%$ for $E_\nu = 1000$ MeV. Moreover, in this case the agreement with the result of

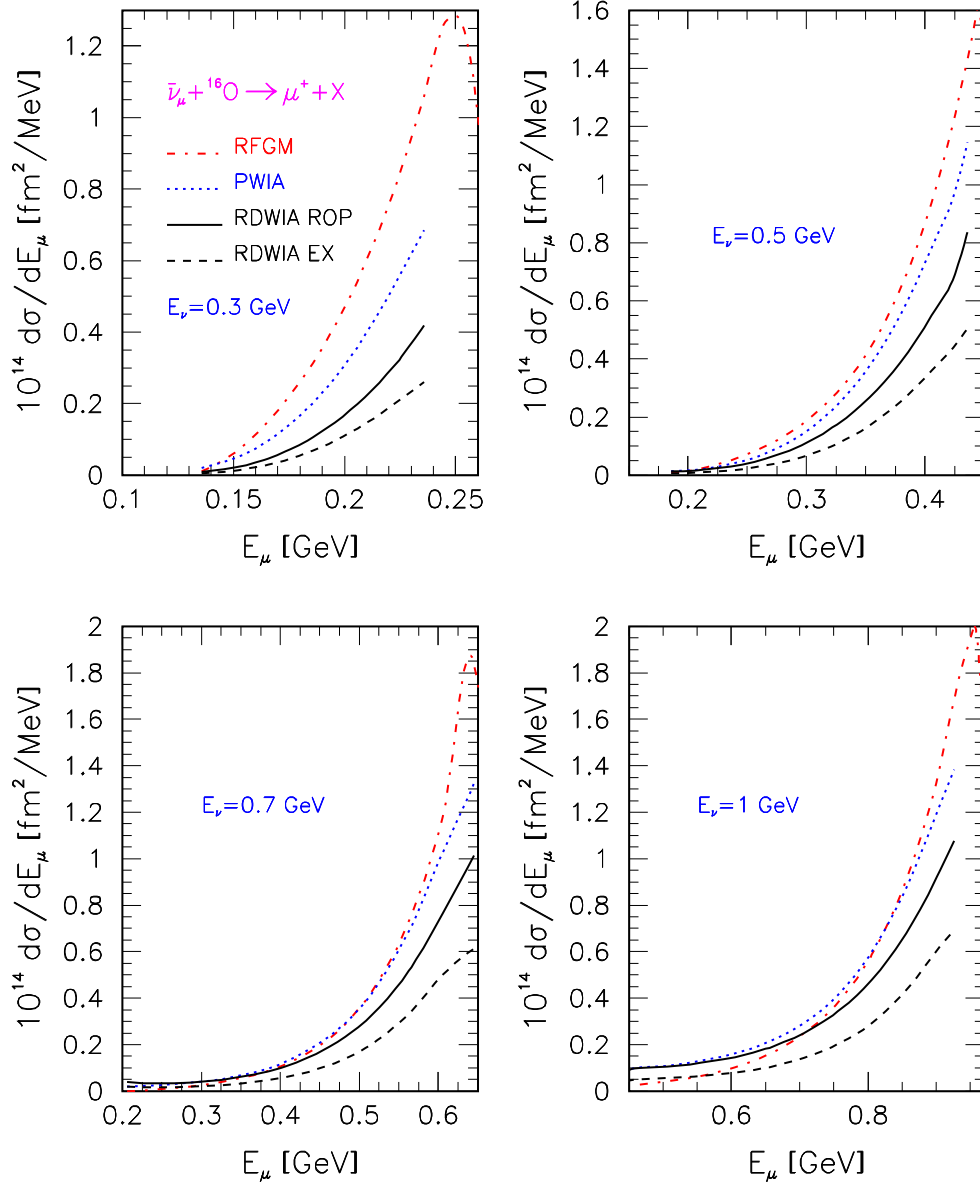


FIG. 9: (Color online) Same as Fig. 8, but for antineutrino scattering.

Ref.[13] is good, and the discrepancy is less than $\pm 6\%$ for $E_\nu > 300$ MeV.

The neutrino and antineutrino total cross sections calculated up to neutrino energy 2.5 GeV are shown in Fig. 11 together with data of Refs.[48–51]. Also shown are the results obtained in the RFGM and PWIA as well as the contribution of the exclusive channels to the total cross sections. The cross sections are scaled with the neutron/proton number in the target. The ratio between the neutrino cross sections calculated in the RFGM and RDWIA ROP decreases with neutrino energy from about 1.5 for $E_\nu = 300$ MeV to ≈ 1.18 for $E_\nu = 1$ GeV and down to ≈ 1.05 for $E_\nu = 2.4$

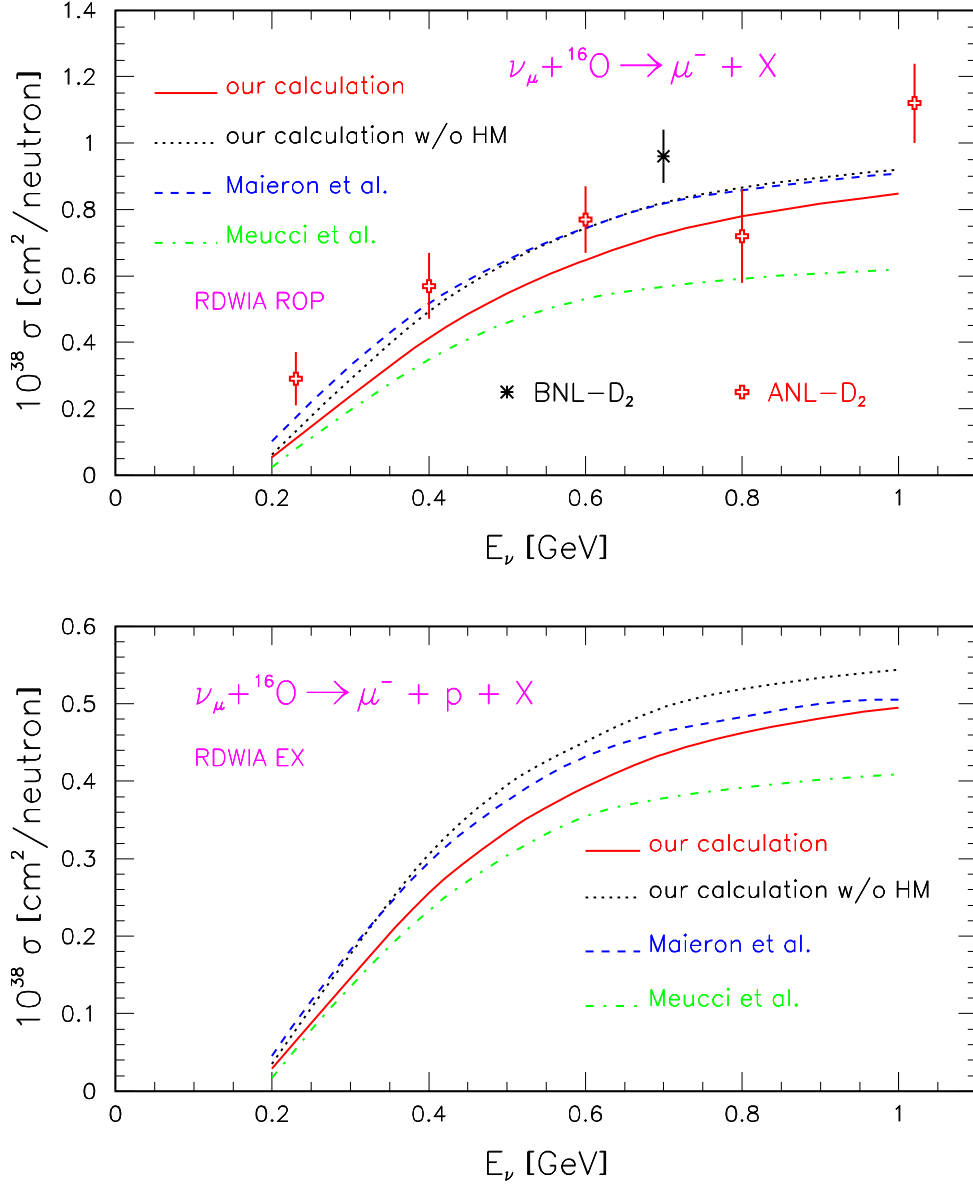


FIG. 10: (Color online) Total cross section for the CC QE scattering of muon neutrino on ^{16}O as a function of the incoming neutrino energy. The RDWIA results with the real part of optical potential (upper panel) and complex optical potential (lower panel) are shown together with calculations from Meucci *et al.* [11] and Maieron *et al.* [13]. The results obtained in this work were calculated with and without the contribution of the high-momentum component. For comparison, data for the D_2 target are shown from Refs.[48, 49].

GeV. For the antineutrino cross sections, this ratio is about 2.7 for $E_\nu = 300$ MeV, 1.3 for $E_\nu = 1$ GeV, and 1.1 for $E_\nu = 2.4$ GeV.

It follows from the comparison of the PWIA and RDWIA results that the FSI effects reduce the total cross section. For the neutrino interactions, this reduction is about 16% for $E_\nu = 300$

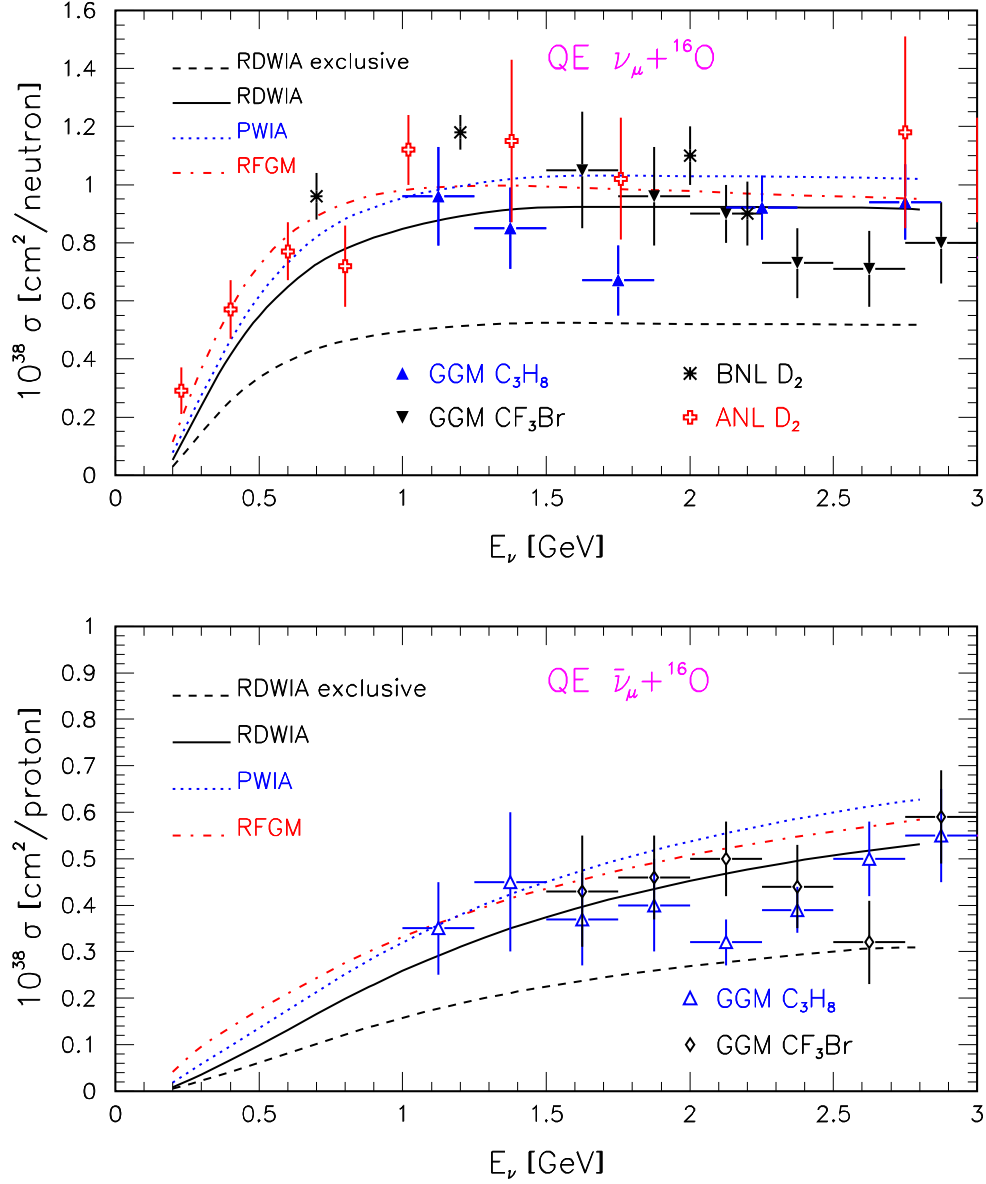


FIG. 11: (Color online) Total cross section for CC QE scattering of muon neutrino (upper panel) and antineutrino (lower panel) on ${}^{16}\text{O}$ as a function of incoming (anti)neutrino energy. Data points for different targets are from Refs.[48–51].

MeV and decreases slowly to 10% for $E_\nu = 2.4$ GeV. The reduction of the antineutrino cross section is about 38% for $E_\nu = 300$ MeV and $\approx 15\%$ for $E_\nu = 2.4$ GeV. We, therefore, observe the weakening of FSI effect in total cross sections with the increase of energy transfer, in accordance with the calculation of Ref.[52]. The contribution of the exclusive channels is about 60%. The results presented in Fig. 11 show significant nuclear-model dependence for energy less than 1 GeV.

V. CONCLUSIONS

In this paper, we study electron and CC quasi-elastic (anti)neutrino scattering on the oxygen target in different approximations (PWIA, RDWIA, RFGM) placing particular emphasis on the nuclear-model dependence of the results. In RDWIA, the LEA program, adapted to neutrino interactions, was used to calculate the differential and reduced exclusive cross sections. This approach was earlier applied to electron-nucleus scattering and successfully tested against data. We found that the reduced cross sections for (anti)neutrino scattering are similar to those of electron scattering, and the latter are in a good agreement with electron data. In calculating the inclusive and total cross sections, the imaginary part of relativistic optical potential was neglected and the effect of NN correlations in the target ground state was taken into account. This approach was tested against electron-oxygen inclusive scattering data; there was overall agreement with the data, with the differences between calculated and measured cross sections in the peak region less than 10%. For neutrino interactions the FSI effect reduces the total cross section by about 30% for $E_\nu=200$ MeV compared to PWIA and decreases with neutrino energy down to 10% at 1 GeV. The effect of NN correlations reduces the total cross section by about 15% at $E_\nu=200$ MeV and also decreases with neutrino energy down to about 8% at 1 GeV.

We tested the RFGM against electron-oxygen scattering data and found that this model does not reproduce the exclusive cross section data. The RFGM also leads to an overestimated value of the inclusive $^{16}\text{O}(e, e')$ cross section at low momentum transfer. The discrepancy is about 20% and decreases as momentum transfer increases. The values of the (anti)neutrino cross sections calculated in this model are also higher than the corresponding values in the RDWIA approach.

We conclude that the data favor the RDWIA results. This indicates that the use of RDWIA in Monte Carlo simulations of neutrino detector response would allow one to reduce the systematic uncertainty in neutrino oscillation parameters.

Acknowledgments

The authors greatly acknowledge communications with J. J. Kelly whose LEA code for nucleon knockout by electron scattering was adapted in this work for neutrino interactions. This work was partially supported by Russian Foundation for Basic Research, Project Nos. 06-02-16353, 06-02-16659, and 05-02-17196.

APPENDIX A: HADRONIC TENSOR AND CROSS SECTION OF EXCLUSIVE ELECTRON AND NEUTRINO SCATTERING

A general structure of the hadronic tensor can be derived from the requirements of Lorentz invariance, parity, and time reversal symmetries. For unpolarized nucleon and a nucleus in the final state, this tensor must be constructed from three linearly independent four-vectors q , p_x , and p_A , the scalars that can be constructed from them, the second-rank metric tensor $g_{\mu\nu}$, and completely antisymmetric tensor $\epsilon_{\mu\nu\alpha\beta}$. Generally, because of the final state interaction effects, the scattered flux at infinity involves complicated asymptotic configurations, and the time reversal symmetry does not constraint the form of the nuclear tensor for the exclusive reactions [28–30].

1. Electron scattering

For electron scattering, the electromagnetic current conservation requires $q_\mu W^{\mu\nu} = W^{\mu\nu} q_\nu = 0$. Taking into account the parity conservation, the nuclear tensor can then be written as a sum of symmetric, $W_S^{\mu\nu(el)}$, and antisymmetric, $W_A^{\mu\nu(el)}$, parts [31]

$$W^{\mu\nu(el)} = W_S^{\mu\nu(el)} + W_A^{\mu\nu(el)}, \quad (\text{A1a})$$

$$W_S^{\mu\nu(el)} = W_1^{(el)} \tilde{g}^{\mu\nu} + W_2^{(el)} \tilde{p}_x^\mu \tilde{p}_x^\nu + W_3^{(el)} \tilde{p}_A^\mu \tilde{p}_A^\nu + W_4^{(el)} (\tilde{p}_x^\mu \tilde{p}_A^\nu + \tilde{p}_x^\nu \tilde{p}_A^\mu), \quad (\text{A1b})$$

$$W_A^{\mu\nu(el)} = W_5^{(el)} (\tilde{p}_x^\mu \tilde{p}_A^\nu - \tilde{p}_x^\nu \tilde{p}_A^\mu), \quad (\text{A1c})$$

where

$$\tilde{g}^{\mu\nu} = g^{\mu\nu} + \frac{q^\mu q^\nu}{Q^2}, \quad (\text{A2a})$$

$$\tilde{p}_x^\mu = p_x^\mu + \frac{p_x \cdot q}{Q^2} q^\mu, \quad (\text{A2b})$$

$$\tilde{p}_A^\mu = p_A^\mu + \frac{p_A \cdot q}{Q^2} q^\mu. \quad (\text{A2c})$$

In target rest frame, the coordinate system is chosen such that the z axis is parallel to the momentum transfer $\mathbf{q} = \mathbf{k}_i - \mathbf{k}_f$ and the y axis is parallel to $\mathbf{k}_i \times \mathbf{k}_f$, and the components of the four-vectors are $k_f = (\varepsilon_f, |\mathbf{k}_f| \sin \theta \cos \varphi, |\mathbf{k}_f| \sin \theta \sin \varphi, |\mathbf{k}_f| \cos \theta)$, $q = (\omega, 0, 0, |\mathbf{q}|)$, $p_A = (m_A, 0, 0, 0)$, $p_x = (\varepsilon_x, |\mathbf{p}_x| \sin \theta_x \cos \phi, |\mathbf{p}_x| \sin \theta_x \sin \phi, |\mathbf{p}_x| \cos \theta_x)$, where θ , φ are lepton scattering angles and θ_x , ϕ are the outgoing nucleon angles.

The lepton tensor for unpolarized electron scattering is symmetric, and therefore the result of contraction of the electron and nuclear response tensors reduces to the form

$$L_{\mu\nu}^{(el)} W_S^{\mu\nu(el)} = 4\varepsilon_i \varepsilon_f \cos^2 \frac{\theta}{2} (V_L R_L^{(el)} + V_T R_T^{(el)} + V_{LT} R_{LT}^{(el)} \cos \phi + V_{TT} R_{TT}^{(el)} \cos 2\phi), \quad (\text{A3})$$

where

$$V_L = Q^4/q^4, \quad (\text{A4a})$$

$$V_T = \frac{Q^2}{2q^2} + \tan^2 \frac{\theta}{2}, \quad (\text{A4b})$$

$$V_{LT} = \frac{Q^2}{q^2} \left(\frac{Q^2}{q^2} + \tan^2 \frac{\theta}{2} \right)^{1/2}, \quad (\text{A4c})$$

$$V_{TT} = \frac{Q^2}{2q^2}, \quad (\text{A4d})$$

are the electron coupling coefficients, and

$$R_L^{(el)} = W^{00(el)}, \quad (\text{A5a})$$

$$R_T^{(el)} = W^{xx(el)} + W^{yy(el)}, \quad (\text{A5b})$$

$$R_{LT}^{(el)} \cos \phi = - \left(W^{0x(el)} + W^{x0(el)} \right), \quad (\text{A5c})$$

$$R_{TT}^{(el)} \cos 2\phi = W^{xx(el)} - W^{yy(el)}, \quad (\text{A5d})$$

are four independ response functions, which describe the electromagnetic properties of the hadronic system.

2. Neutrino scattering

In weak interactions, the weak current and parity are not conserved. Therefore, a general nuclear tensor can be written as

$$W^{\mu\nu(cc)} = W_S^{\mu\nu} + W_A^{\mu\nu}, \quad (\text{A6a})$$

$$\begin{aligned} W_S^{\mu\nu} = & W_1 g^{\mu\nu} + W_2 q^\mu q^\nu + W_3 p_x^\mu p_x^\nu + W_4 p_A^\mu p_A^\nu + W_5 (p_x^\mu q^\nu + p_x^\nu q^\mu) \\ & + W_6 (p_A^\mu q^\nu + p_A^\nu q^\mu) + W_7 (p_x^\mu p_A^\nu + p_x^\nu p_A^\mu), \end{aligned} \quad (\text{A6b})$$

$$\begin{aligned} W_A^{\mu\nu} = & W_8 (p_x^\mu q^\nu - p_x^\nu q^\mu) + W_9 (p_A^\mu q^\nu - p_A^\nu q^\mu) + W_{10} (p_x^\mu p_A^\nu - p_x^\nu p_A^\mu) \\ & + W_{11} \epsilon^{\mu\nu\tau\rho} q_\tau p_{x\rho} + W_{12} \epsilon^{\mu\nu\tau\rho} q_\tau p_{A\rho} + W_{13} \epsilon^{\mu\nu\tau\rho} p_{x\tau} p_{A\rho}. \end{aligned} \quad (\text{A6c})$$

Note that because of Hermiticity of $W^{\mu\nu(cc)}$, each term of $W_S^{\mu\nu}$ must be real, while each term of $W_A^{\mu\nu}$ must be imaginary, and $L_{\mu\nu}^{cc} W^{\mu\nu(cc)}$ is real. The result of contraction of the lepton and nuclear tensors can be written as

$$\begin{aligned}
L_{\mu\nu}^{(cc)} W^{\mu\nu(cc)} = & L_{\mu\nu}^S W_S^{\mu\nu} + L_{\mu\nu}^A W_A^{\mu\nu} = 2\varepsilon_i \varepsilon_f \{ v_0 R_0 + v_T R_T + v_{TT} R_{TT} \cos 2\phi + v_{zz} R_{zz} \\
& + (v_{xz} R_{xz} - v_{0x} R_{0x}) \cos \phi - v_{0z} R_{0z} + h[v_{yz}(R'_{yz} \sin \phi + R_{yz} \cos \phi) \\
& - v_{0y}(R'_{0y} \sin \phi + R_{0y} \cos \phi) - v_{xy} R_{xy}] \}, \tag{A7}
\end{aligned}$$

where

$$v_0 = 1 + \beta \cos \theta, \tag{A8a}$$

$$v_T = 1 - \beta \cos \theta + \frac{\varepsilon_i \beta |\mathbf{k}_f| \sin^2 \theta}{q^2}, \tag{A8b}$$

$$v_{TT} = \frac{\varepsilon_i \beta |\mathbf{k}_f| \sin^2 \theta}{q^2}, \tag{A8c}$$

$$v_{0z} = \frac{\omega}{|\mathbf{q}|} (1 + \beta \cos \theta) + \frac{m_l^2}{|\mathbf{q}| \varepsilon_f}, \tag{A8d}$$

$$v_{zz} = 1 + \beta \cos \theta - 2 \frac{\varepsilon_i |\mathbf{k}_f| \beta}{q^2} \sin^2 \theta, \tag{A8e}$$

$$v_{0x} = (\varepsilon_i + \varepsilon_f) \frac{\beta \sin \theta}{|\mathbf{q}|}, \tag{A8f}$$

$$v_{xz} = \frac{\beta}{q^2} \sin \theta [(\varepsilon_i + \varepsilon_f) \omega + m_l^2], \tag{A8g}$$

$$v_{xy} = \frac{\varepsilon_i + \varepsilon_f}{|\mathbf{q}|} (1 - \beta \cos \theta) - \frac{m_l^2}{|\mathbf{q}| \varepsilon_f}, \tag{A8h}$$

$$v_{yz} = \beta \frac{\omega}{|\mathbf{q}|} \sin \theta, \tag{A8i}$$

$$v_{0y} = \beta \sin \theta, \quad \beta = |\mathbf{k}_f| / \varepsilon_f, \tag{A8j}$$

are neutrino coupling coefficients, and

$$R_0 = W_S^{00}, \tag{A9a}$$

$$R_T = W_S^{xx} + W_S^{yy}, \tag{A9b}$$

$$R_{TT} \cos 2\phi = W_S^{xx} - W_S^{yy}, \tag{A9c}$$

$$R_{0z} = W_S^{0z} + W_S^{z0}, \tag{A9d}$$

$$R_{zz} = W_S^{zz}, \tag{A9e}$$

$$R_{0x} \cos \phi = W_S^{0x} + W_S^{x0}, \tag{A9f}$$

$$R_{xz} \cos \phi = W_S^{xz} + W_S^{zx}, \tag{A9g}$$

$$R_{xy} = i (W_A^{xy} - W_A^{yx}), \tag{A9h}$$

$$R'_{yz} \sin \phi + R_{yz} \cos \phi = i (W_A^{yz} - W_A^{zy}), \tag{A9i}$$

$$R'_{0y} \sin \phi + R_{0y} \cos \phi = i \left(W_A^{0y} - W_A^{y0} \right), \quad (\text{A9j})$$

are ten independ response functions which describe the weak properties of the hadronic system.

In the absence of FSI effect (plane-wave limit) the nucleon flux conserves in exclusive reaction. For this reason, the time reversal symmetry of operators and states provides an additional constraint on the Lorenz form of the antisymmetric part of nuclear tensor (A6c), in particular, the structures like $a^\mu b^\nu - a^\nu b^\mu$ (with a and b four-momenta) vanish. Then we have

$$W_A^{\mu\nu} = W_{11} \varepsilon^{\mu\nu\tau\rho} q_\tau p_{x\rho} + W_{12} \varepsilon^{\mu\nu\tau\rho} q_\tau p_{A\rho} + W_{13} \varepsilon^{\mu\nu\tau\rho} p_{x\tau} p_{A\rho} \quad (\text{A10})$$

and

$$\begin{aligned} L_{\mu\nu}^{(cc)} W^{\mu\nu(cc)} = 2\varepsilon_i \varepsilon_f \{ & v_0 R_0 + v_T R_T + v_{TT} R_{TT} \cos 2\phi + v_{zz} R_{zz} + (v_{xz} R_{xz} - v_{0x} R_{0x}) \cos \phi \\ & - v_{0z} R_{0z} + h(v_{yz} R_{yz} \cos \phi - v_{0y} R_{0y} \cos \phi - v_{xy} R_{xy}) \}, \end{aligned} \quad (\text{A11})$$

where

$$R_{yz} \cos \phi = i \left(W_A^{yz} - W_A^{zy} \right), \quad (\text{A12a})$$

$$R_{0y} \cos \phi = i \left(W_A^{0y} - W_A^{y0} \right). \quad (\text{A12b})$$

Note that the response functions R'_{yz} and R'_{0y} are related to W_{8-10} terms which vanish in the plane-wave limit. It follows from the expressions (A7) and (A11) that the cross sections asymmetry, which is measured at azimuthal angles $\phi = \pi/2$ and $\phi = -\pi/2$, vanishes in the absence of the FSI.

-
- [1] S. Hatakeyama *et al.* (Super-Kamiokande Collaboration), Phys. Rev. Lett. **81**, 2016, 1998; M. Ambrosio *et al.* (MACRO Collaboration), Phys. Lett. **B434**, 451, 1998; W. W. Allison *et al.* (Soudan-2 Collaboration), Phys. Lett. **B449**, 137, 1999.
 - [2] Y. Fukuda *et al.* (Super-Kamiokande Collaboration), Phys. Rev. Lett. **81**, 1562, 1998; Erratum-ibid. **81**, 4279, 1998; B. T. Cleveland *et al.*, Astrophys. J. **496**, 505, 1998, W. Hamlet *et al.* (GALLEX Collaboration), Phys. Lett. **B447**, 127, 1999; J. N. Abdurashitov *et al.* (SAGE Collaboration), Phys. Rev. **C60**, 055801, 1999.
 - [3] B. Aharmim *et al.* (SNO Collaboration), Phys. Rev. **C72**, 055502, 2005; Y. Ashie *et al.* (Super-Kamiokande Collaboration), Phys. Rev. **D71**, 112005, 2005.
 - [4] T. Araki *et al.*, Phys. Rev. Lett. **94**, 081801, 2005.
 - [5] M. H. Ahn *et al.*, Phys. Rev. **D74**, 072003, 2006.

- [6] D. G. Michael *et al.*, Phys. Rev. Lett. **97**, 191801, 2006.
- [7] G. P. Zeller, arXiv:hep-ex/0312061.
- [8] A. V. Butkevich and S. P. Mikheyev, Phys. Rev. **C72**, 025501, 2005.
- [9] *Modern Topics in Electron Scattering*, edited by B. Frois and I. Sick (World Scientific, Singapore, 1991).
- [10] O. Benhar and D. Meloni, Nucl. Phys. **A789**, 379 (2007).
- [11] A. Meucci, C. Giusti, and F. D. Pacati, Nucl. Phys. **A739**, 277, 2004.
- [12] A. Meucci, C. Giusti, and F. D. Pacati, Nucl. Phys. **A744**, 307, 2004.
- [13] C. Maieron, M. C. Martinez, J. A. Caballero, and J. M. Udias, Phys. Rev. **C68**, 048501, 2003.
- [14] M. C. Martinez, P. Lava, N. Jachowicz, J. Ryckebusch, K. Vantournhout, and J. M. Udias, Phys. Rev. **C73**, 024607, 2006.
- [15] J. Nieves, J. E. Amaro, and M. Valverde, Phys. Rev. **C70**, 055503, 2004.
- [16] E. Kolbe, K. Langanke, S. Krewald, F. K. Thielemann, Nucl. Phys. **A540**, 599, 1992.
- [17] C. Vople, N. Auerbach, G. Colo, T. Suzuki, N. Van Giani, Phys. Rev. **C62**, 015501, 2000.
- [18] N. Jachowicz, K. Heyde, J. Ryckebusch, S. Rombouts, Phys. Rev. **C65**, 025501, 2002.
- [19] S. K. Singh, Nimai C. Mukhopadhyay, E. Oset, Phys. Rev. **C57**, 2687, 1998.
- [20] J. J. Kelly, <http://www.physics.umd.edu/enp/jjkelly/LEA>
- [21] J. J. Kelly, Phys. Rev. **C72**, 014602, 2005
- [22] J. Gao *et al.*, Phys. Rev. Lett. **84**, 3265, 2000
- [23] K. G. Fissum *et al.*, Phys. Rev. **C70**, 034606, 2004
- [24] J. J. Kelly, Phys. Rev. **C71**, 064610, 2005
- [25] S. Frullani and J. Mougey, Adv. Nucl. Phys. **14**, 1 (1984).
- [26] C. Ciofi degli Atti and S. Simula, Phys. Rev. **C53**, 1689, 1996.
- [27] S. A. Kulagin and R. Petti, Nucl. Phys. **A765**, 126, 2006.
- [28] A. Picklesimer, J. W. Van Orden, S. J. Wallace, Phys. Rev. **C32**, 1312, 1985.
- [29] A. Picklesimer, J. W. Van Orden, Phys. Rev. **C35**, 266, 1987.
- [30] T. W. Donnelly and A. S. Raskin, Ann. Phys. **169**, 247, 1986.
- [31] J. J. Kelly, Adv. Nucl. Phys. **23**, 75, 1996.
- [32] T. de Forest, Nucl. Phys. **A392**, 232, 1983.
- [33] P. Mergell, U.-G. Meissner, and D. Drechsel, Nucl. Phys. **A596**, 367, 1996.
- [34] J. J. Kelly, Phys. Rev. **C59**, 3256, 1996
- [35] C. Horowitz and B. Serot, Nucl. Phys. **A368**, 503, 1981.
- [36] M. M. Sharma, M. A. Nagarajan, and P. Ring, Phys. Lett. **B312**, 377, 1993.
- [37] M. Leuschner *et al.*, Phys. Rev. **C49**, 955, 1994
- [38] J. M. Udias, P. Sarriguren, E. Moya de Guerra, E. Garrido, and J. A. Caballero, Phys. Rev. **C51**, 3246, 1995.
- [39] M. Hedayati-Poor, J. I. Johansson, and H. S. Sherif, Phys. Rev. **C51**, 2044, 1995.
- [40] E. D. Cooper, S. Hama, B. C. Clark, and R. L. Mercer, Phys. Rev. **C47**, 297, 1993.

- [41] A. Meucci, F. Capuzzi, C. Giusti, and F. D. Pacati, Phys. Rev. **C67**, 054601, 2003.
- [42] L. Chinitz *et al.*, Phys. Rev. Lett. **67**, 568, 1991.
- [43] M. Bernhein *et al.*, Nucl. Phys. **A375**, 381, 1982.
- [44] M. Leuschner *et al.*, Phys. Rev. **C49**, 955, 1994.
- [45] L. L. Schiff Phys. Rev. **103**, 443, 1956.
- [46] J. S. O'Connell *et al.*, Phys. Rev. **C35**, 1063, 1987.
- [47] M. Anghinolfi *et al.*, Nucl. Phys. **A602**, 402, 1996.
- [48] W. A. Mann *et al.*, Phys. Rev. Lett. **31**, 844, 1973.
- [49] N. J. Baker *et al.*, Phys. Rev. **D23**, 2499, 1981.
- [50] M. Pohl *et al.*, Lett. Nuovo Cim. **26**, 332, 1979.
- [51] J. Brunner *et al.*, Z. Phys. **C45**, 551, 1990.
- [52] Y. Horikawa, F. Lenz and Nimai C. Mukhopadhyay, Phys. Rev. **C22**, 1680, 1980.